Observing Simulated Images of the High Redshift Universe: The Faint End Luminosity Function

by

Robert Morgan

A Dissertation Presented in Partial Fulfillment
of the Requirements for the Degree
Doctor of Philosophy

Approved April 2012 by the
Graduate Supervisory Committee:

Rogier Windhorst, Chair
Evan Scannapieco
James Rhoads
Carl Gardner
Andrei Belitsky

ARIZONA STATE UNIVERSITY

May 2012

ABSTRACT

Numerical simulations are very helpful in understanding the physics of the formation of structure and galaxies. However, it is sometimes difficult to interpret model data with respect to observations, partly due to the difficulties and background noise inherent to observation. The goal, here, is to attempt to bridge this gap between simulation and observation by rendering the model output in image format which is then processed by tools commonly used in observational astronomy.

Images are synthesized in various filters by folding the output of cosmological simulations of gasdynamics with star-formation and dark matter with the Bruzual-Charlot stellar population synthesis models. A variation of the Virgo-Gadget numerical simulation code is used with the hybrid gas and stellar formation models of Springel and Hernquist (2003). Outputs taken at various redshifts are stacked to create a synthetic view of the simulated star clusters. Source Extractor (SExtractor) is used to find groupings of stellar populations which are considered as galaxies or galaxy building blocks and photometry used to estimate the rest frame luminosities and distribution functions. With further refinements, this is expected to provide support for missions such as JWST, as well as to probe what additional physics are needed to model the data.

The results show good agreement in many respects with observed properties of the galaxy luminosity function (LF) over a wide range of high redshifts. In particular, the slope (alpha) when fitted to the standard Schechter function shows excellent agreement both in value and evolution with redshift, when compared with observation. Discrepancies of other properties with observation are seen to be a result of limitations of the simulation and additional feedback mechanisms which are needed.

DEDICATION

To the loving memory of my parents Bob and Carrie, and the support of my wife, Jena.

ACKNOWLEDGEMENTS

I am grateful to the ASU Advanced Computing Center (A2C2) for their generous allotment of computer time and assistance for the simulations.

Also, to Rob Thacker for initial conditions file and the Virgo P-Gadget simulation code. I would also like to thank my adviser, Rogier Windhorst, for his many suggestions and advice. A special thanks to Evan Scannapieco for his many hours of discussion and analysis and for the idea of converting numerical simulation results into observational-like image files, which is the principal theme for this work. I would also thank James Rhoads for his helpful suggestions.

TABLE OF CONTENTS

LIST OF TABLES

LIST OF FIGURES

LIST OF SYMBOLS/NOMENCLATURE

FITS - Flexible Image Transport System - a common image/data file format system used in astronomy.

Gpc - Gigaparsec, One billion (one thousand million) parsecs (see pc.)

h - The Hubble constant in dimensionless units, = H0/100km/sec/Mpc

Mpc - Megaparsec, One million parsecs (see pc.)

pc - parsec, a unit of astronomical distance, approximately 3.5 light years

z - letter used for value of the redshift

PREFACE

Astronomy differs from most of the traditional sciences in that it is mostly limited to observation, idue to the large scales involved in distance, energy and time. Astronomy must rely mostly on observation. Of course, one attempts to connect observation with known physics such as thermodynamics, gravitation, electromagnetism, particle physics and chemistry. Even knowing physics and chemistry, there are still many unknowns, such as how the first stars formed and what were they like; what were their masses, how long did they last? Similarly, the formation and history of the first galaxies is still a mystery in many ways.

Of course, many theories have been put forward, many with much success. But, it is not always easy to match theory with observation. In part, this is due to the problems with observation, especially as we look into the distant past. There is dust and gas and scattered star light which limits our ability to see details, even with the largest space based instruments available now or for the foreseeable future.

There are several, and some controversial, thoughts on the role of simulation. These range from being just a solver for intractable analytical problems, to being somewhere between experiment and theory, to even a new kind of science (Wolfram 1985.) It is not sought to settle these issues here, but does suggest that adding realistic views and images to simulation output, to visualizing the data in a manner subject to the tools and methods of observational astronomers can add to the interpretation of models and the interaction between theory and observation.

INTRODUCTION

Here I explore the usefulness of combining traditional image processing techniques in observational astronomy with numerical cosmological simulations. Previously, some authors (e.g., Nakamine (2007) and many others) have coupled simulations with stellar population synthesis models such as the Bruzual-Charlot models, (Bruzual-Charlot 2003, hereafter BC03) to obtain Spectral Energy Distributions (SED's) for stellar populations. Overzier et al. (2012) are working on a similar project to produce images from semi-analytic simulations.

I use this method of producing synthetic images in FITS formats from the SEDs in selected infrared (IR) filter bands to obtain luminosity functions in the rest-frame UV band. Initially, minimal background sky noise is added to assist the image analysis program Source Extractor (SExtractor), but still preserve most details of the simulation structure. Later, more realistic noise levels are added to see how these artifacts affect the interpretation and “observation” of the model.

Further, the numerical simulations combine dark matter and baryonic physics. While dark matter simulations provide the initial scaffolding for building structure, baryons are needed to dissipate energy and momentum to allow compact objects to form. While more computationally intensive, this simplifies the assumptions in the model and avoids semi-analytic models, which have been criticized for the number of assumptions.

Chapter 1

OVERVIEW

This section describes the analysis of numerical simulations with methods and tools commonly used by observational astronomers. The outputs of the simulations are converted into image files, which can then be processed by tools such as Source Extractor (SExtractor, Bertin and Arnouts 1996), and to include effects such as realistic sky backgrounds. By using established Spectral Emission Distribution (SED) fitting models such as Bruzual-Charlot (2003, BC03) and filters such as WFC3 (Wide Field Camera 3), the goal is to create images that capture sufficient astronomical information and may be manipulated by usual observational methods and yield useful astronomical information.

Images are synthesized at high redshift from a cosmological numerical simulation including both dark and baryonic matter. The numerical simulation is from a version of Gadget2 including gas hydrodynamic SPH, heating and cooling from Katz et al. (1996) and star-formation (Springel & Hernquist,2003, hereafter SH03) and used in the Virgo simulation, with permission from Rob Thacker, who also supplied the inirial conditions particle files. The model uses a hybrid gas/star particle model, which has cool gas, hot gas and star components. Star “particles” are formed from the hybrid gas particles, representing a stellar population, or massive star complexes.

Stellar population ages and metallicities are extracted from the simulation data and loaded into the Bruzual-Charlot 2003 (hereafter BC03) stellar population models to obtain a spectral energy distribution (SED) of the simulated stellar population. The Padova (1994) models (BC03) using the Chabrier Initial Mass Function (IMF) are used. The SED is folded with a filter response function from the BC03 filter library to obtain an observed luminosity which is converted into a flux using the luminosity

distance using the LCDM model parameters. The fluxes and spatial coordinates from the simulation are converted into FITS (Flexible Image Transport) files, creating images of the stellar population at given redshifts and filters.

Standard image processing tools, such as SExtractor are used to analyze this simulated universe. One intention is to develop a tool for simulating high redshift images to assist in planning for and interpreting observations for missions such as the planned James Webb Space Telescope (JWST).

The Gadget model writes data files of the states of each model particle to files, which are referred to as “snapshots,” at times (redshifts) which are given in a table written by the user. The times were given corresponding to the “light crossing” times (18 Mpc/h/((1+z)*c), where z is the redshift value and c is the speed of light, for the simulation cube, which was defined as 18 comoving Mc/h. Initially, it was planned to write a data snapshot for each light crossing time, but this was too data storage expensive, so every other time (i.e., two light crossings) was used. The following diagrams provide an overview of the processing pipeline:

- The Numerical Simulation
- Extract Star “Particle” Data
- Calculate Integrated Fluxes with BC03 models
- Create Synthetic Image Files and process w/SExtractor
- Extract Luminosity Functions (LFs), Analyze Data

The letters indicate steps in the process, referred to in the verification chapter.

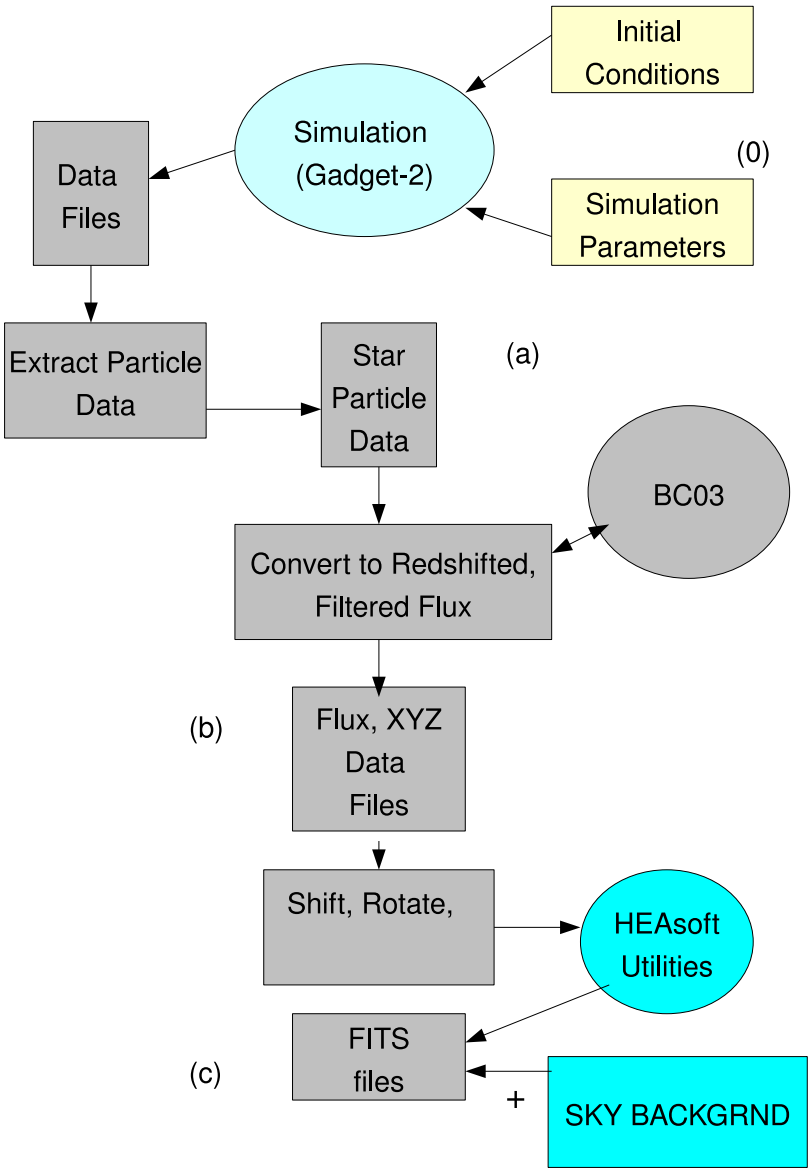

Figure 1.1: Overview of Process to Create
Images from Simulation Star Data

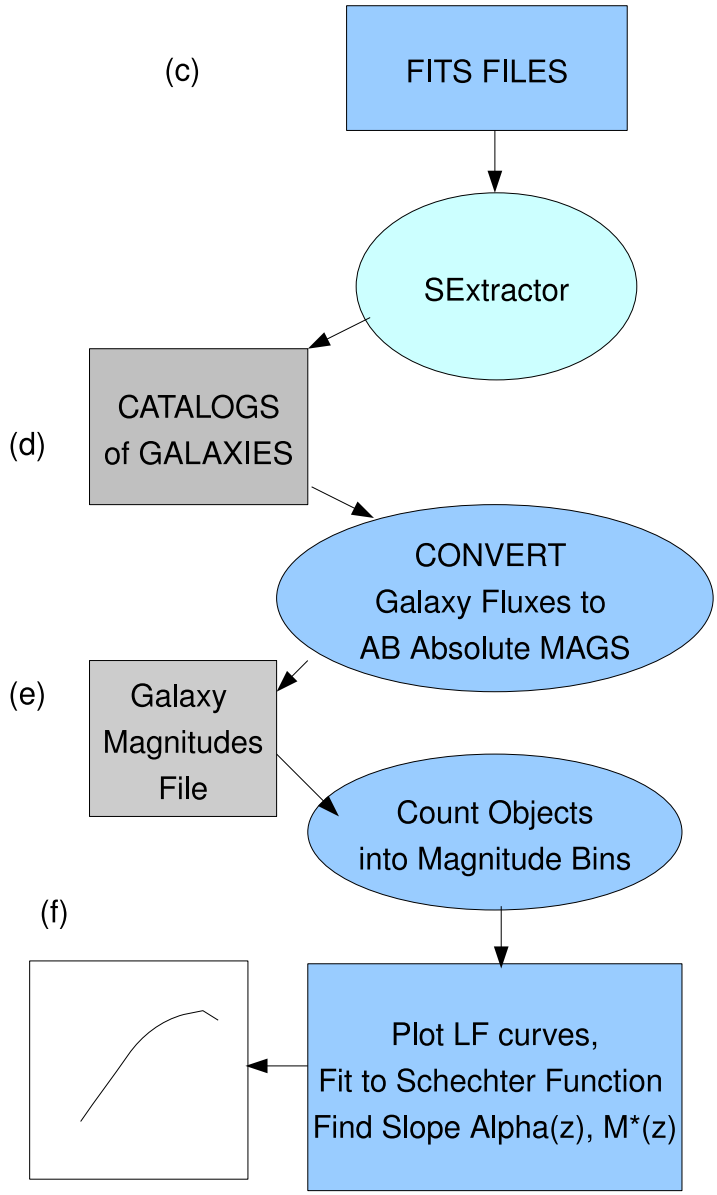

Figure 1.2: Overview of End Process to Analyze
FITS Images from Simulation Star Data

Chapter 2

SIMULATION

Initial conditions were supplied by R. Thacker as a set of files containing positions and velocity values of both dark matter and baryons (gas particles) at a redshift of z = 199 (scale factor a = 0.005.) The numerical simulations were run on 512 nodes of the super-computing cluster at Arizona State University named “Saguaro” (Arizona Advanced Computing Center or A2C2). The simulation volume was a periodic cube of 18 comoving Mpc/h size on a side, where h = H_0/100 km/sec/Mpc. The simulation used 2 x 512^3 particles, with an equal number of dark matter and gas particles, on a 1024 grid. Cosmological LCDM values used were H_0 = 71.9, Ω_Λ = 0.724, and Ω_b = 0.0441, giving a baryon mass resolution of 5.4 x 10^5 $M_\odot$/particle. Note that a slightly different value for Ω_Λ was used, 0.73, for the calculation of distances, due to newer information from the WMAP project. However, this does not affect the restframe absolute magnitude.

The numerical simulation code is from a variant of Gadget2 (P-Gadget2) used in the Virgo Gadget project, excluding certain proprietary codes. It includes gas hydrodynamic SPH, heating and cooling from Katz et al. (1996) and star-formation (Springel & Hernquist, 2003, hereafter SH03). A “hybrid” gas/star particle model, which has cool gas, hot gas and star components, is used. Star “particles” are formed from the hybrid gas particles, representing a stellar population, when 50% of the hybrid particle has been converted to stars. An entropic formulation is used which helps prevent the overcooling in other numerical models. The star formation is controlled by a single parameter, the star formation time scale.

“Snaphots” (binary files of particle data) were written at time intervals corresponding to two light crossing times of the simulation cube. The star-formation

code creates “stars” in the multi-phase gas particles when a sufficient fraction of the gas reaches appropriate temperature and density conditions (SH03). A “star particle” is formed from a gas particle when 50% of the mass is in the stellar phase. Thus, the “star” particles are of mass 2.7 x 10^5 $M_\odot$. The particle data files were processed to extract data on the “star particles”, including mass, metallicity and formation time, which was used to obtain rest frame SEDs using the BC03 models, previously described.

2.1 Feedback - “Winds”

The simulation was also run with the ”WINDS” parameter on. This is a feature in SH03 that attempted to incorporate feedback in the form of supernovae driven ”winds” in the gas clouds surrounding the star clusters. When turned on, part of the energy of a supernova (SN) would impart a velocity ”kick” to the multi-phase gas particle (i.e., part of a star forming molecular cloud) along the axis of rotation of the cloud. This was an attempt to simulate the gas stripping effects of SN on gas clouds caught in shallow potential wells of smaller dark matter haloes. Also, a time delay was set so that the particle would not interact with other gas particles until it had traveled a set distance - the mean free path of the particles, or 50 million years had passed, whichever was shorter.

The parameters for this simulation are given in the following table.

Parameter	Value	Comments (see SH2003)
WindEfficiency	0.5	1/eta = 2.0
WindEnergyFraction	0.25	chi in SH2003 4.1, p.296 (Wind carries x fraction of super nova (SN) energy)
WindFreeTravelLength	0.5	0.5 kpc/h
WindFreeTravelDensFac	0.1	see SH2003 p.299, end of 5.4

Table 2.1: Simulation “WINDS” Parameters.

Chapter 3

METHODOLOGY

3.1 Introduction

In this section, it is described in detail:

• How star particle data are extracted from model snapshot files.

• How this data is processed by the BC03 models to create a simulated observed flux.

• Conversion of this flux to synthetic image files.

• Processing of the image files by SExtractor to find collections or groupings, putting into catalogs.

• Reduction of the catalog data to find source restframe absolute magnitudes, producing Luminosity Functions (LF's).

• Statistical Analysis and fitting of the LF's to Schechter functions, and analyzing for LF evolution.

Also discussed, is the rationale for the selection of the pixel scale for the FITS files, hence, the image scale of the star particles, relative to the inherent physical size of the simulated objects, the resolution of the instruments, current and planned. The instruments here are considered space based, though land based instruments could be included if comparable resolution scales could be achieved.

3.2 Data Extraction

In order to ensure reliable code, the code supplied in Gadget to read the snapshot files was used. The user interface code, written in IDL (Interactive Data Language) was converted to “C” language code for portability. to “C.” The code which actually read the snapshot files was already written in “C”, and was modified only to allow the ectra fields in the simualtion and to accomodate the larger memory requirements. This permitted the code greater portability, such as running on the Saguaro computer cluster, since it did not require the IDL package present.

3.3 Interface to BC03

The star particle files, described above, were read by a “C” program. The metallicity data were mappped with a table lookup to the appropriate metallicity model in BC03. The star age was calculated using a table of cosmic age developed for this system. The cosmic age of the formation (i.e., “birth”) of the star particle and the redshift of the particle snapshot data (i.e., the time of the “galaxy”) were subtracted to give the age of the star particle relative to the the simulated observed galaxy. This information was used in a table lookup to see if the particular metal-age table were in memory, on disc, or if the BC03 program “galaxevpl” needed to be called to generate the table.

In the following sections are described how the SED table information was used to synthesize a “virtual CCD camera” count for the simulated pixel for the star particle. By keeping tables in memory, and adding new tables when they were needed, throughputs on the order of several thousand flux calculations per second were achieved on an ordinary Linux desktop computer.

3.4 Flux & Magnitudes

The initial wavelength range is found by “blue-shifting” the observed filter range back to the emitted restframe. Note that since the endpoints are blue-shifted, this narrows the emission band compared with the detected band. As luminosity in the BC03 models is expressed in units of $L_{\odot}^{-1}M_{\odot}^{-1}$ Å^{-1} , this is multiplied by the star particle mass in Mt$\odot$ and the solar luminosity in Joules m^{-2} to facilitate the later conversion to a count in the ”virtual” CCD.

Since the wavelengths are stretched by the redshift, the energy density per unit wavelength, in the observer’s frame, is reduced by a factor 1+z, representing the change in energy density per unit time in an expanding universe. After being redshifted to the observed frame, and divided by 4 Pi times the luminosity distance squared, this gives an energy flux density per unit wavelength. This is then convolved with the filter response function by stepping through each interval in the redshifted SED and the filter response function, taking the product and checking for when either the SED or filter response step changes. This gives an integrated flux.

To get the total energy, this flux is then multiplied by a factor (10^{13}) representing the product of the telescope aperture (area A) and the exposure time (t). For this virtual instrument, this is nominally taken to be a JWST class instrument. While this value may be high, it is later reduced by an appropriate factor when taking the sky background (BG) into account. It is high here in order to maintain a high S/N ratio, since later processing requires some, though small, noise to be added and it is desired to examine the model output in detail, as a baseline.

In a real CCD instrument, an incoming photon count is converted to electrons which is then converted by an analog to digital unit (ADU) to a count, which is recorded. To mimic this process, the energy is converted to units of Joules, and

divided by 10^{-19}, approximately the energy (the ”work function”), needed to produce an electron from a CCD. Since the attempt is not to exactly simulate in detail any particular instrument, the exact factors are unimportant, provided the scales are consistent eith the values used in introducing background noise. Also, to use the same factors when calculatiing an apparent magnitude of the synthesized objects, discussed later.

This gives an ”electron count” N_e , where f is the total integrated flux and the telescope aperture given by area A, for an exposure time (t):

$$\text{Count} = N_e = A * t * f / 10^{-19} \text{ Joules}$$

The incident flux f is given by:

$$f = L/(4\pi D_L^2) \quad ,$$

where D_L = the luminosity distance (the comoving distance times (1+z))

When observed through a filter with bandpass BP, the observed integrated flux is given by:

$$F_{BP} = \int F(\lambda/(1+z),t(z)) R(\lambda) (1+z)^{-1} d\lambda \ ,$$

where $F(\lambda)$ is the incident flux and $R(\lambda)$ is the filter response function.

The factor of $(1+z)^{-1}$ comes from redshift “stretching” of the emitted wavelength range. If simulating an actual instrument, a term OTA (optical telescope assembly) would be included for the effect of the telescope structure, mirror figure and, if multiple mirrors or segments were used, such as in JWST, the geometry of such segments. However, at this time, no specific instrument is modeled, though such could be added. Note, however, that the environment is included by adding different levels of sky background. Also, while some work has been done in post-processing the flux with a point spread function (PSF), some of that effect is accounted for in the SExtractor image filter mask. The one used has a FWHM value of 2 pixels, or 0.2

arcseconds for the image scale used here (see discussion under image and pixels scales, later.)

The count value is then recorded in a file, along with the object's comoving coordinates in a "flux-position" file, which is then converted to an image file in FITS format by processing (all discussed later.)

3.5 Magnitude Calculations

To compute an apparent magnitude in the AB system, the total energy count needs to be converted to a flux per unit frequency. The integrated flux is divided by the artificial aperture and time constant above, converting energy units to ergs, and dividing by the filter effective width in Hz to obtain f_ν in ergs s^{-1} cm^{-2} Hz^{-1}.

The AB magnitude is obtained using the formula (Oke & Gunn 1983) $m_{AB} = -2.5\log(f_u) - 48.60$, where f_ν is in ergs s^{-1} cm^{-2} Hz^{-1}. To convert to an absolute M_{AB} magnitude in the rest frame emitted band use:

$$M_{AB} = m_{AB} - 5\log(D_{L/Mpc}) - 25 + 2.5\log(1+z) \quad (3)$$

where D is the luminosity distance and $2.5\log(1+z)$ is the k-correction which results from the redshift "stretching" of the emission band. It is positive since magnitudes are computed in the frequency domain (Hogg, et al. 2002), whereas in the prior calculation of the total apparent "observed" energy, the calculation was in the wavelength domain since the SED and filter responses were in $Å^{-1}$. The calculation of the absolute magnitude is done on the photometric catalog produced by SExtractor when detecting "objects" clusters of star particles which are taken to be galaxies in formation (discussed more later.)

3.6 Filter Selection

In order to compare these results with recent results by Hathi et al. (2010), it is necessary to choose filters which are consistent with restframe emissions in the 150 nm. band. The criteria used here is that used by Dahlen et al. (2007), in that the restframe emission, 150 nm here, should be between the first and third quartile range of the integrated flux of the chosen filter band in the restframe of the emission. (See the following chart.)

z\Filter	***Gunn i***	***Gunn z***	***Y WFC3***	***J Johnson***	***same***	***H Bessel & Brett***	***same***
Rest frame (z=0)							
Eff λ (nm)	809	920	1059	1249	1249	1646	1646
1st Quartile	765	870	987	1160		1600	
3rd Quartile	855	975	1131	1360		1740	
redshifted							
redshift (z)	4.52	5.32	6.00	7.16	7.68	9.50	10.90
Eff λ	146.6	145.6	151.1	153.1	143.9	156.8	138.3
diff(150nm)	-3.40	-4.40	1.10	3.10	-6.10	6.80	-11.70
1st Quartile	138.6	137.7	140.8	142.2	133.6	152.4	134.5
3rd Quartile	154.9	154.3	161.4	166.7	156.7	165.7	146.2

Table 3.1: Effective wavelengths and response functions of selected filters with respect to 150 nm emission.

3.7 Image and Pixel Scales

This section describes the creation of image files , in Flexible Image Transport (FITS) format, for processing by SExtractor. As previously described, the fluxes of the star particles in filter bands were computed according to the metallicity and age of the simulated star particles, using the BC03 models and the luminosity distance. The

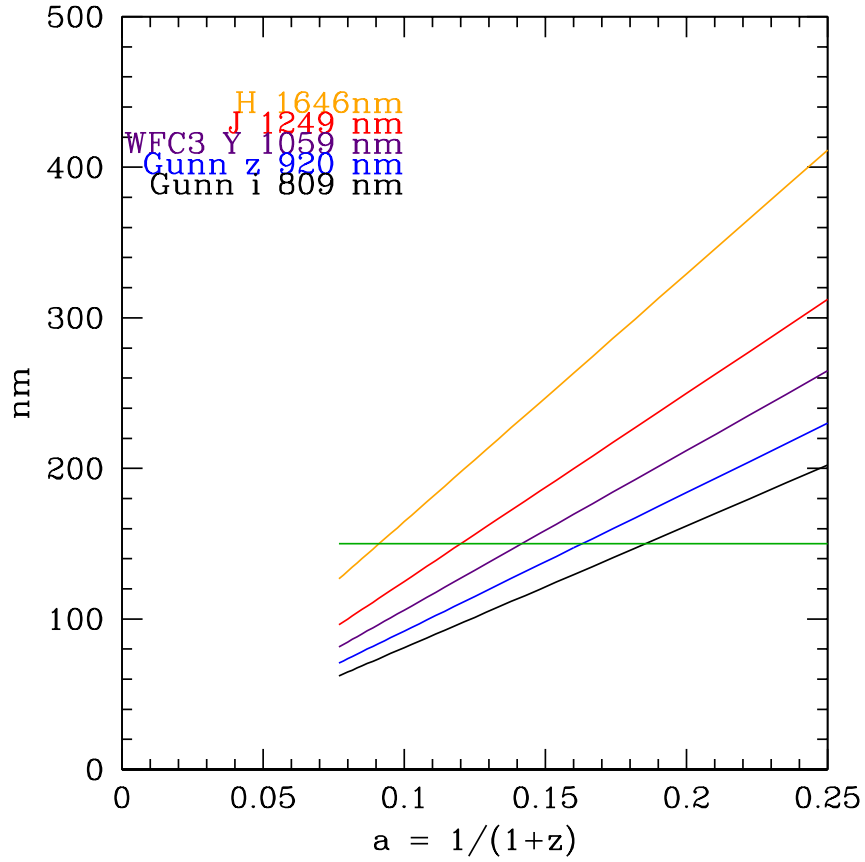

Figure 3.1: Effect of redshift on emission wavelength;
Scale factor (1/(1+z)) for 150 nm emission.

redshifted flux is integrated with the filter response, multiplied by the the simulated aperture and exposure time and recorded in a file, along with the comoving coordinates for the particle. This file (the 'flux-position" file), after some spatial transforms to be described shortly, is then recorded as in a FITS file using publicly available HEAsoft (High Energy Astrophysics Group) software utility. Each particle is represented by a single pixel in this image file, with the integrated flux count as the value of the pixel.

The size of the FITS frame and position of the pixels in the frame is determined by the geometry of the LCDM parameters and the redshift of the snapshot used to make the frame. This is most easily computed in comoving coordinate space.

Each frame is sized relative to its angular projection in comoving space from a solid angle through z=3.0, with a resolution of 8192 x 8192 pixels. That is, a CCD of 8192 x 8192 pixels is simulated with an instrument that has a field of view (FOV) such that at a redshift of z = 3.0, an area of sky corresponding to a square 18 Mpc/h on a side would precisely fit on that CCD. This redshift was chosen as that was the target for the end of the simulation. However, the simulation became very slow below reshift 5.0, so the runs were terminated at a redshift of 4.5.

Hence, each frame is projected on a reference frame at z = 3 according to a line-of-sight projection relative to the observer at z = 0. In comoving flat space, the inverse square law holds. As an example, a snapshot at a comoving distance at twice the reference distance, would be half the size on each side, or 4096 x 4096 pixels (see figure xx.)

The scale chosen is a compromise between storage requirements, the resolution of instruments such as HST and JWST and the size of the represented objects: super massive star complexes (SMSC's) and star forming regions at the mass resolution of the simulation ($2.7 \times 10^5 M_\odot$) discussed below. The FITS files take about 100 megabytes (MB) of storage at a redshift of z =9 to about 200-300 MB at redshift 6 and lower, depending upon the filter. In addition, there are fits files formed by stacking multiple FITS files at different redshifts and combining with different simulated sky noise “flats,” and FITS files adjusted for different exposure times to match a given sky noise for a desired S/N ratio. Since a number of different filters were used, this represents a significant storage requirement, especially at the start of this project.

For the chosen LCDM model for distance calculation (H_0 = 71.9, Omega = 0.73), the comoving distance at z = 3.0 is 6.4 Gigaparsecs (Gpc), giving an angular scale of 30.9 kpc per arcsecond in comoving coordinates, or 7.73 kpc, in proper

coordinates, per arcsecond. This pixel subtends an arc of ˜0.099 arcsecond. Note that the angular scale is preserved across all redshifts.

At a more typical redshift of z = 6, the comoving distance is 8.3 Gpcs, giving a pixel scale of 410 comoving parsecs (pc), or 580 pc in proper size. At z =9, the pixel scale is about 450 proper pc. A star particle in this simulation is about 2.7 x 10ˆ5 solar masses. If we consider these star particles that have formed out of a gas particle to be super star clusters or SSC's, this size is not unreasonable (C. Herrera, 2012.)

Matching the physical scale in this resolution is the primary consideration, since we cannot resolve on a finer scale, even if we increased the pixel count. Fortunately, this scale approximates the Hubble WFC3 resolution (0.12 arcseconds/pixel,NASA webpage) and is not too far from the proposed JWST instrument.

Each individual cube is relatively thin at the observer's distance (18 Mpc/h ˜0.003 of the comoving distance at z = 6), so perspective is not included within an individual frame. The individual particles are projected on a plane perpendicular to the observer (the "sky".) The cube is taken to be orientated so that one axis is pointing towards the observer (more on this later.) This introduces a small distortion, but also recall that the simulation is occurring in the same time, not on the space-time "cone" as would appear to a real observer, so there is an inherent difference between the model and "real" space-time.

That is, for a real observer the front of the cube would be at a lower redshift than or +- 0.38 % at z =3. At z = 6, this difference in z is +- 0.029, for an error of 0.48%. This introduces an uncertainty in the flux and "observed" magnitudes. (Make table .)

Note that in the case of stacked images, if nothing were done, an aliasing

problem would occur since snapshots are taken of the same simulation at different times in the cosmic evolution. One method to avoid this would be to do different simulations with different initial conditions for each snapshot. However, this becomes very computationally expensive. A way out of this dilemma is through the nature of the simulation being a periodic box. By this, it is meant that the simulation box has periodic boundary conditions. It is as if the simulation were in a 3-D hall of mirrors, extending to infinity in all directions perpendicular to the cube's surfaces, with a periodic repetition, except that mirror inversion. Also, particles exiting through one surface reappear on the other side, so there is have conservation of matter and energy. Note that this is because in the periodic conditions, the particle about to exit also exists ”outside” the box, moving toward the box boundary from the other side.

Thus, “other” (virtual) cubes in this periodic space can be selected to be the “next” cube in simulation time. Further, the cube can be randomly oriented along the x-y-z axes by cyclically and randomly permuting the x-y-z orientation (i. e., [x, y, z] -> [y,z,x] or ->[z, x, y].) Then the positions are mapped onto the new x'y' plane and shifted by a random amount between 0.0 and 18.0 in the x' and y' coordinates, the arithmetic being modulo 18 (Mpc/h), such that 17.0 + 3.0 = 2.0. Basically, one is just selecting random 18 Mpc/h cubes out of the infinite periodic space to be the next spatial volumes looking back along the line of sight of the simulated observation.

3.8 Image Processing - SExtractor

The randomly translated files of flux and sky-projected coordinates were translated into FITS files using a “HEAsoft” (High Energy Astrophysics Group) list to FITS file utility and sized as previously described.

The FITS source frame or, if a range of images were used, the merged frames were combined with a simulated poisson distributed sky noise background FITS file.

Initially, the program ”DS9” was used to “smooth” the pixels with a gaussian kernel, but over concerns that this might affect the photometry, a convolution mask was employed in SExtractor to distribute the star particle flux over the nearby area. This is necessary since gas particles and radiative transfer are not currently incorporated in the images and it is necessary to simulate an extended object for SExtractor to detect and select as an object. Thus, it is necessary to have flux above the sky background in adjacent pixels for the SExtractor detection phase to consider a group of particles as an ”object”, or galaxy. Without this, SExtractor would ”see” these pixels as isolated objects, possibly identifying them as foreground stars.

Various parameters were used to extract source objects and inspect the sensitivity of the results to those parameter selections. This is a difficult problem since we have two main independent sources of error - the simulation itself and the selection criteria used for SExtractor. A gaussian convolution mask of 5 x 5 pixels with a full width half maximum (FWHM) of 2.0 pixels was used. This enables star-particles which are near each other, but not “touching”, to be seen as part of a single object.

The SExtractor object selection is discussed further in the section on ”completeness” in the chapter on ”Verification.”

3.9 Sky Background

The initial minimalist poisson background mask yielded a sky background of ~ 39 magnitudes per square arcsecond for the filters simulated here. This is orders of magnitude better than HST and JWST, and meant to produce the maximum detail from the model. It was needed because SExtractor requires some amount of background to execute. SExtractor automatically performs sky subtraction, and complains if there is no background. Since this provides the maximum information from the model output, it is needed as a baseline with which to compare results when

Redshift (z)	Comoving distance (Gpc)	pixels	Comoving size (kpc/”)	Proper size (kpc/”)
3	6.38	8192	30.93	7.73
4	7.22	7239	35.00	7.00
5	7.84	6666	38.01	6.33
6	8.32	6282	40.34	5.76
7	8.71	6001	42.23	5.28
9	9.31	5614	45.14	4.51

Table 3.2: Distance and Image Scale as function of Redshift

more realistic sky backgrounds are added, to see if that observing artifact affects the results. i.e. the parameters of the fitted Schechter function. This is described as “No Sky Bg” in the results.

To simulate real sky conditions, noise masks were used with mean counts of 10^6 per pixel or 10^8 per arcsecond^2. The magnitude values were calculated using the same codes that computed apparent magnitudes from source fluxes in the SExtractor catalogs. This gives a sky background of $\sim$ 22.6 AB magnitudes per arcsecond$\hat{2}$. The image FITS files were adjusted so that this background level would correspond to the ERS data (reference) for that filter. This amounted to shortening the simulated exposure time. Thus, the S/N ratio is not quite constant from filter to filter. This change in the exposure time is denoted by the term ”EXP factor” oe ”EXP” in the tables. Thus, an EXP of 100 would effectively reduce a one year exposure (the nominal time for the ”virtual” instrument for a JWST class aperture) down to about 3.6 days, which is not an unreasonable exposure.

The SExtractor catalogs of selected objects and total fluxes (within a certain radius) were then processed through a program, using the rules previously described, to compute the apparent and absolute magnitudes, using the luminosity distance for that redshift (from a table previously generated) and the filter effective width. These values were written out to a file which was then processed by programs which binned and counted the objects by absolute magnitude and produced luminosity functions and fitted to Schechter functions, to be described in the next section.

Filter	eff λ (nm)	filter width (nm)	BG mag/ sec^2	normalized sky BG (EXP factor)	BG EXP=100 mag/sec^2	BG EXP=300 mag/sec^2	Redshift (no. frames stacked)
i	809		22.5 (22.6)		23.27	22.08	
z	870	96	22.3 (22.6)		22.68	21.48	5.32(1)
Y WFC3	1058	137	22.2 (22.6)	22.60 (115)	22.76	21.56	6.008 (1) 6.24(5)
J	1249	297	22.2 (22.5)	22.53 (194)	23.25	22.06	7.16 (5) 7.68 (5)
H	1646	283	21.7 (22.3 at 1541 nm)	22.30 (130)	22.59	21.40	9.5 (5) 10.38 (5) 10.9 (5)
K	2195	578	N/A (22.3) (at 1541 nm)		22.75	21.56	
NIRCam F356W	3559	764			22.00	20.81	

Table 3.3: Sky Background (BG) levels. More realistic space sky background (BG) levels – 10^6 counts/pixel, Background (BG) first column data from Windhorst, et al. (2010), parentheses () from Windhorst, et al. (2011)

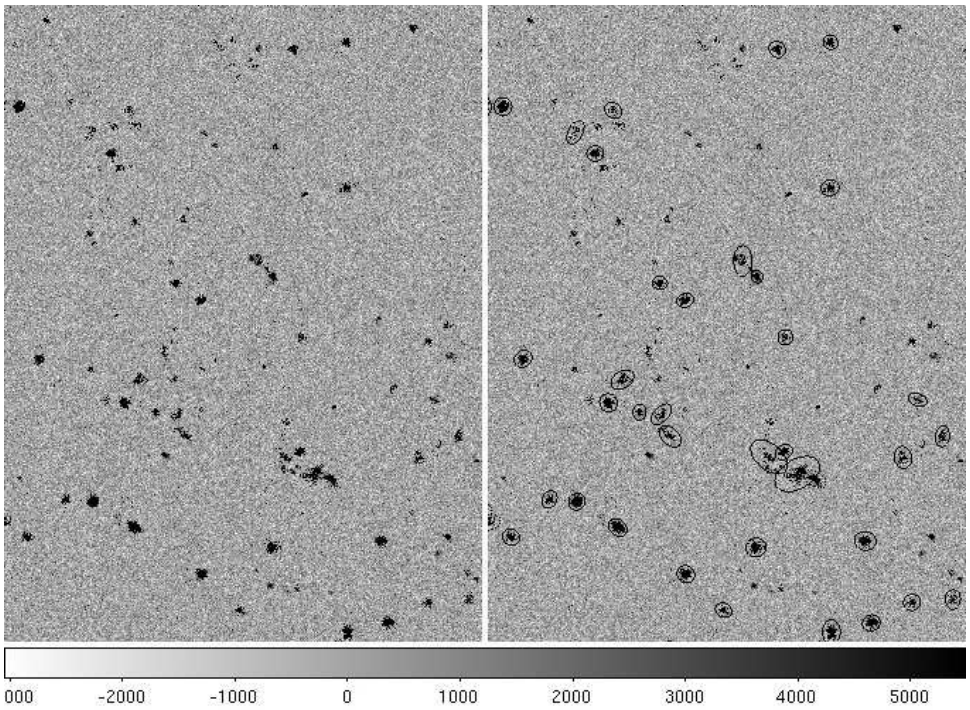

Figure 3.2: FITS file and Check Image file output
from SExtractor for z=5.3 through
Gunn z filter (54) with sky background

3.10 Schechter LF Curve Fitting

This section describes the method of fitting the luminosity function (LF) data to a Schechter function, using a least squares (LSQ) method to find best fit parameters. A variable size binning was used in order to maximize the degrees of freedom (dof) and to ensure a minimum count per bin, described below.

The data, which was collected from the output of the SExtractor run (described previously), was converted to restframe absolute magnitudes. The filters in the Bruzual-Charlot flux calculation stage were chosen so that the restframe emission band was approximately 150 nm in order to allow comparison with the Hathi, et al (2010) data. (That comparison is not shown in this section.)

The LF data was fitted to a Schechter function in magnitude space of the form:

$$\Phi(M) = 0.4ln(10) * (\phi_*) * exp(-10^{(-0.4*(M-M*))}) * 10^{[(-0.4)(\alpha+1)(M-M*)]} \quad (3.1)$$

where M is the absolute magnitude, and M$*$ is the characteristic magnitude obtained by substituting M - M$*$ = -2.5 log(L/L$*$) in the luminosity form of the function.

Φ(M) is the volume density count of objects of magnitude M, with M $*$, alpha and the normalization $\Phi*$ as free parameters. The fitting here is in the absolute AB magnitude parameter space, using a least squares minimization of the chi square function:

$$\chi^2 = \Sigma(Y_i - y_i(\theta))^2 / y_i(\theta), \quad (3.2)$$

where Y_i are measured values and $y_i(\theta)$ are the expected or predicted values for parameters θ, which here are M$*$, α and $\phi*$. The expectation or predictor function is the Schechter function, which uses the product of a power law and exponential function to predict the volume number density of objects (e.g., galaxies) within a magnitude range versus magnitude. The free parameters are the characteristic magnitude M$*$, where the exponential function breaks, the slope alpha of the power law, and the normalization value.

The minimization technique used was essentially a brute force calculation over a broad range of the parameter space ($-33.9 \leq M \leq 16.9$ with 500 steps and $-2.4 \leq \alpha \leq -1.0$ with 150 steps), calculating the sum of the residuals for each combination of the parameters. For each selected value of M$*$ and alpha, a more dynamic fitting was used to minimize chi square for the normalization parameter. The code ”zoomed in” (took smaller steps) when the chi square value fell below a specified threshold value and then to exit the loop over normalization parameter space when the chi square value exceeded a threshold after reaching a minimum for that region of

parameter space. This method was checked against a less dynamic, but slower search, and found accurate. This search was performed in IDL (Interactive Data Language.) The contours of constant chi square values in the parameter space are also shown. Contours were drawn for three confidence levels (i.e, 0.68, 0.90, and 0.99), found by adding an appropriate increment (2.30, 4.61, and 9.21, respectively) to the best fit minimum chi square value (Practical Statistics for Astronomers, Wall and Jenkins, 2003). Contour plots are included below.

The fits were also performed by varying parts of the parameter space, namely the maximum absolute magnitude. This was necessary since the LF dropped off steeply at faint magnitudes, generally around mag AB 16.0 with minimal sky noise ($\sim 40 magAB$) and at $\sim$ 18.0 for realistic sky background ($\sim 23 mAB$). This dropoff is apparently a completness effect from a combination of the model resolution (the minimum object mass, 10 star particles, is 2.7 x $10^6 M\odot$) and the effect of background noise.

The bin magnitude was chosen as the numeric average over the magnitudes for each object in the bin. The width was nominally 0.25 magnitude. However, since the LSQ fit is unreliable for small counts, a minimum count (10) was selected for each bin. This affected only the brightest bins, since the total count was in the 1000's, even greater than 10,000 in some cases. Also, in order to improve resolution and increase the degrees of freedom, a maximum count (100 or 50 depending upon the total object count) was also chosen. The objects were sorted by absolute magnitude, and the bin terminated when the count reached the maximum value. If the maximum was not reached by the time the bin size reached 0.25 magnitude, the bin was terminated then.

The uncertainty for each parameter $M*$ and alpha, was found by projecting orthogonally the one sigma contour onto each parameter axis. In practice, this amounted to a search in the $M*$ - alpha parameter space for chi square values bracketing the one sigma (0.68) values described above. The chi square values computed in the search were captured in an array of minimal chi square values for each $M*$, alpha pair. The minimum was found by searching over $\phi*$ - the normalization. This was also the space used to draw the contours.

Chapter 4

VERIFICATION

Comparisons were made between the AB magnitudes computed through the programs described above against results independently obtained using the BC03 program "zmag," in order to verify correctness of this important phase of the measuring process. The "zmag" utility allows one to compute the magnitude (Vega or AB), in a given filter, of a "galaxy", or, in this case, a star "particle" with a given metallicity and an age in Gigayears (Gyrs) since it was formed. Referring to the process diagrams, this tests steps (a) to (b) and (d) to (e). Additional tests were also made to verify the correctness of (b) to (d), at least for single star particles.

A filter in the BC03 filter set is specified, including any that may have added by the user, and the redshift at which the galaxy or star particle is observed. It is desired to compare the restframe magnitude calculated from the synthesized redshifted and filtered flux, with the "zmag" restframe of the star particle in the corresponding restframe filter. For this partof the test, we set z=0, and the filter selected to be the nearest to the restframe emission band of the stellar population being tested.

The test is to compare a test population of the same age and metallicity at a large redshift and through a filter (IR to far IR) corresponding to the redshifted emission restframe with the restframe population. This computes a count as previously described. This count (flux) is processed by the system to compute the restframe absolute AB magnitude. This value is then compared to the AB absolute magnitude obtained through the BC03 "zmag" utility.

This provides an independent verification of the entire end-to-end flux/magnitude/red and blue shifting code. To be more precise, the test includes:

1) Obtaining the SED of a stellar population of metallicity Z and age t

2) Selecting the correct restframe wavelength range of that SED at redshift z for filter F

3) Redshifting that SED range correctly to the observers frame (z=0) 4) Convolving that flux with the filter F's response function, converting to a flux count.

5) Taking that count, reversing the calculations, and finding the restframe AB magnitude of the test stellar population.

In order to obtain the rest-frame emission, the observer is effectively transported to the time and place of the light emission by setting the redshift in “zmag” to 0 and the galaxy (stellar) age as the age at the emitted time. Then, the nearest rest-frame filter band is selected as the zmag filter. When the difference between the emitted effective wavelength (the “blue-shifted” observer frame filter) and the filter used for the zmag z=0 AB magnitude calculation was small, the difference in magnitudes was negligible, validating the magnitude calculations in the pipeline.

Two types of tests were performed. In one, the redshift is set so that emitted wavelength precisely corresponds to the “observed” filter effective wavelength after redshift. This is a test of how accurately the set of programs perform in finding the emitted portion of the SED, then redshifting that part and convolving with the filter, and then reconstructing the rest frame AB magnitude. Note that, since the filter bandwidths and response functions of the emitted UV or B filter and the redshifted observed IR filters will differ, even though the effective wavelengths are matched, there is expected to be some difference. However, it is desired that this be as small as possible. This is seen in the table below.

In the second case, since we cannot always have a perfect match between restframe emission and IR filters, we wish to see the magnitude difference as a function of the wavelength discrepancy, even though we apply the criteria in Dahlen et al. (2010).

Age Gyrs	AB Mag Z = 0.02 z=6.48	AB Mag Z = 0.02 z=0 (zmag)	difference (zmag - pgm)
0.709	7.714	7.770	0.056
0.679	7.390	7.442	0.052
0.614	7.390	7.442	0.052
0.529	6.807	6.849	0.042
0.457	6.517	6.555	0.038
0.381	6.007	6.040	0.033

Table 4.1: Comparison of absolute AB magnitudes of a star population (normalized to one solar mass) between BC03 utility “zmag” and the author’s program. The populations are of different ages, but at solar metallicity.

Age Gyrs	**AB Mag Z = 0.02 z=6.48**	**AB Mag Z = 0.02 z=0 (zmag)**	**difference (zmag - pgm)**
0.709	5.9946	6.0078	0.013
0.679	5.7912	5.8052	0.014
0.614	5.7912	5.8052	0.014
0.529	5.4469	5.4618	0.015
0.457	5.2964	5.3116	0.015
0.381	4.9771	4.9924	0.015

Table 4.2: Same as above, but at metallicity Z = 0.00019 (0.01 solar)

z\ Filter	star age (Gyrs)	H (Bessel & Brett)	K John-son	UV5 (bc03 30)
z		6.01	6.01	0
λ		235	313	332
	0.582	7.090	6.044	5.783
	0.232	5.010	4.573	4.462
	0.132	4.050	3.780	3.73

Table 4.3: Z=6.00 (TBD) AB Magnitudes of simulated stars compared with BC03 “zmag” AB magnitudes of close rest frame bands. All are solar metallicity.

		a	b	c	c2	d	e				
Filter	star age	H	K	L	ST-UV22	UV5	B	a-d	b-d	c-e	a-c2
z		6.24	6.24	6.24	0	0	0				
λ(nm)		227	303	475	220	332	442	105	29	33	7
	0.7512	7.68	6.52	4.37	7.77	6.08	4.55	1.61	0.45	-0.18	-0.09
	0.6733	7.37	6.35	4.24	7.44	5.93	4.41	1.44	0.41	-0.17	-0.07
	0.5715	7.09	6.17	4.11	7.15	5.78	4.27	1.01	0.39	-0.16	-0.06
	0.4998	6.80	5.98	3.99	6.85	5.63	4.14	1.17	0.36	-0.15	-0.05
	0.4237	6.25	5.60	3.77	6.29	5.31	3.89	0.95	0.30	-0.12	-0.04

Table 4.4: Z=6.24. AB Magnitudes of simulated stars compared with BC03 “zmag” AB magnitudes of close rest frame bands. All are solar metallicity.

4.1 Schechter Function Fitting Tests

Artificial LF's were created from Schechter Function models with various parameters of M*, alpha, and normalization. The counts were given a random poisson distribution. These files were then processed as normal luminosity files and attempts made to recover the parameters.

4.2 Completeness Testing

Tests were made comparing SExtractor results with a conventional Friends-of-Friends from the Astronomy Dept. at U. of Washington code on the original particle data set. This was compared to running SExtractor on the same data set after it had been processed through a simulated filter, converted to an image in FITS format and had noise added. Of 1149385 star "particles", SExtractor found 8711 "galaxies" using the criteria given, which required a minimum of 10 objects. The FOF code found 8802 objects for a linking length of 25Kpc and 8987 groups for a linking length of 20Kpc. This corresponds to 99% and 97% respectively, for SExtractor objects vs. FOF groups. Now, this does not define the completeness ratio precisely, nor does it offer a comparison of the relative distributions of the numbers of objects by size, but this test provides a measure of confidence in the use of this method of converting data sets to images and processing by imaging detection tools, such as SExtractor.

Chapter 5

ERROR ANALYSIS

Given a luminosity L and a luminosity distance D_L , the flux F is given by :

$$F = L / 4*\pi D_L^{\,2}$$

Thus, the error in F as a function of the error in D_L , ignoring the luminosity L for the moment, is :

$$\delta F/F = -2 * \delta D_L / D_L$$

For a comoving distance = x, the luminosity distance is $D_L = a * x$, where the scale factor a = (1/1+z), and redshift z. This gives the error $\delta D_L = a * \delta x$, substituting in the equation above :

$$\delta F/F = -2 * \delta x/x$$

Previously, it has been seen that the maximum error within a frame is 12.5/x, where x is measured in Mpc. At z = 6.0, the comoving distance is ˜ 8.3 Gpc, giving $dx/x = 12.5/8.3 \times 10^{-3}$ ˜ 0.15 %, which gives a relative error in the flux dF/F = 0.3 %. At z=9, x = 9.3 Gpc, hence the relative error in flux dF/F = 2 * 12.5/9.3 = 0.27 %. At z = 4, the error is dF/F = 2 * 12.5/7.2 = 0.35 %.

For stacked frames, since every other frame was omitted, this gives a total of n-1 x2 x 25 + 25Mpc = 50n – 25 Mpc comoving distance from front to back, or a maximum of 25n – 12.5 Mpc from the center frame. For n=5, this becomes an error of ±100 Mpc, or 8 times the errors quoted above for a single frame at the given redshifts, or about 2 % average error (taking z = 6 as a typical redshift.)

The magnitude M is given by $M - M_0 = -2.5 * \log(L/L_0) = -2.5 \log(F/F_0)$, for the same distance (10 pc for absolute magnitude), and some reference magnitude M_0. The error in magnitude is $dM = 2.5\ dF/F \sim 0.008$ for single frame (max) or 5% for 5 stacked frames.

Chapter 6

RESULTS

As described previously, model data were processed through the BC03 models and converted into FITS files in various filters in the IR and far IR regions to correspond with restframe emissions at 150 nm (UV) at redshifts in the range of 4.5 to 12ing the criteria previously discussed. This was in order to compare with published observations in the 150nm restframe. These FITS files were combined with sky background (BG) FITS frames to simulate realistic sky noise levels or with minimalist noise to enable processing with SExtractor. Objects were detected and selected by SExtractor. Photometry was also done to obtain total fluxes for the selected objects. The SExtractor catalogs were read and apparent and absolute magnitudes computed for the objects using the comoving distance for the objects redshift. The AB absolute magnitudes were counted and binned by 1/4 magnitude ranges to produce the printed LF curves. Initially, these binning data were written to files for simple power law fitting for the LF slope. Later, variable size binning was done on the object magnitude data processed from the SExtractor catalogs, and Schechter function fitting, with M*, alpha, and normalization as free parameters, was done. Nominally, the bins in this fitting were of 0.1 magnitude in size, although the bins were enlarged to maintain a minimum of 5 counts per bin (most were orders of magnitude larger.) This was due to the unreliability of chi square testing for counts less than 5.

Using the comoving volume (depending upon whether a single or multiple stacked frames were used) the number density per magnitude was computed and results plotted against magnitude as a luminosity function (LF). Results of this, comparing the effects of different sky background levels (previously described) are shown on the following pages.

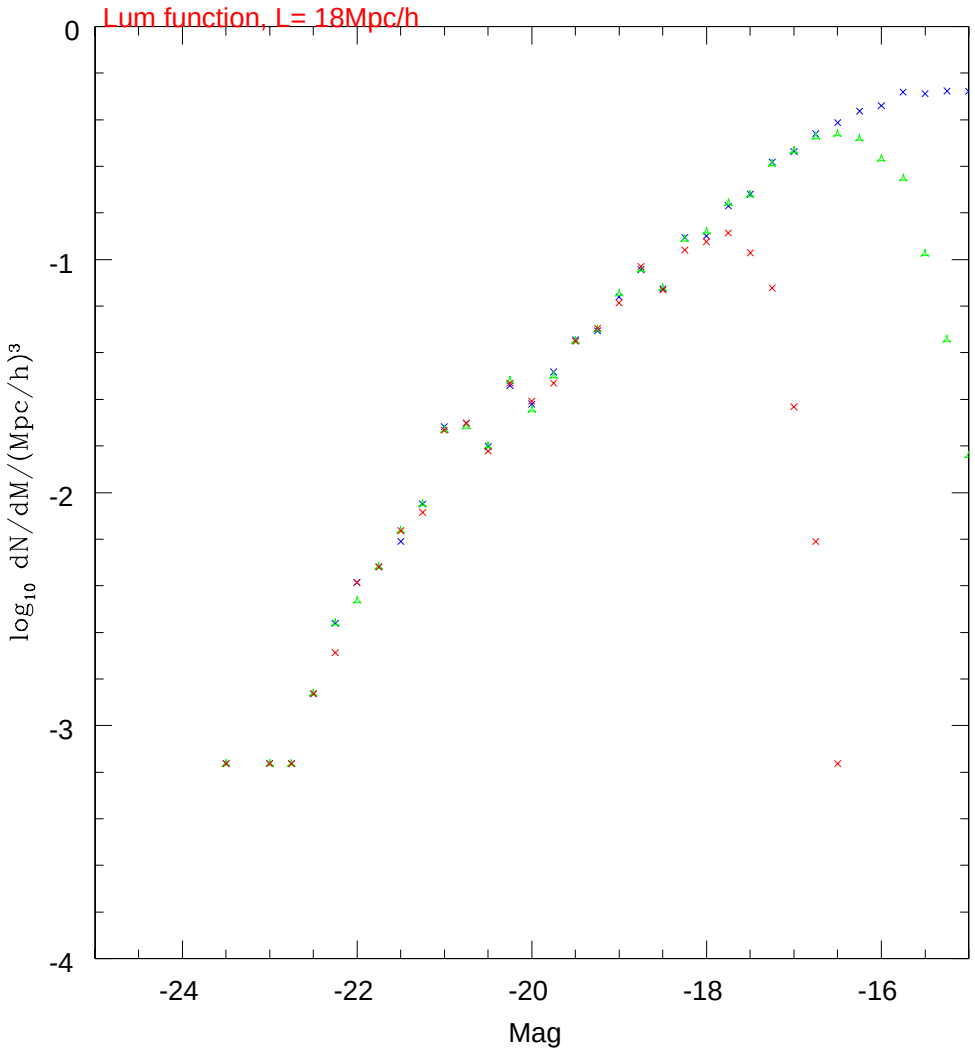

Figure 6.1: LF at redshift 6.01 through simulated WFC3 F105 Filter.

Blue-minimal sky BG (mag 40) ; Green-very small BG (mag 30) ; Red-normal space sky BG (mag 22.6)

6.1 Redshift Evolution of LF Slope Alpha

Comparisons of the uv 150nm range LF are shown with the results of Hathi, et al. 2010. for the range.

The following figures show the simulated LF's derived from the model for

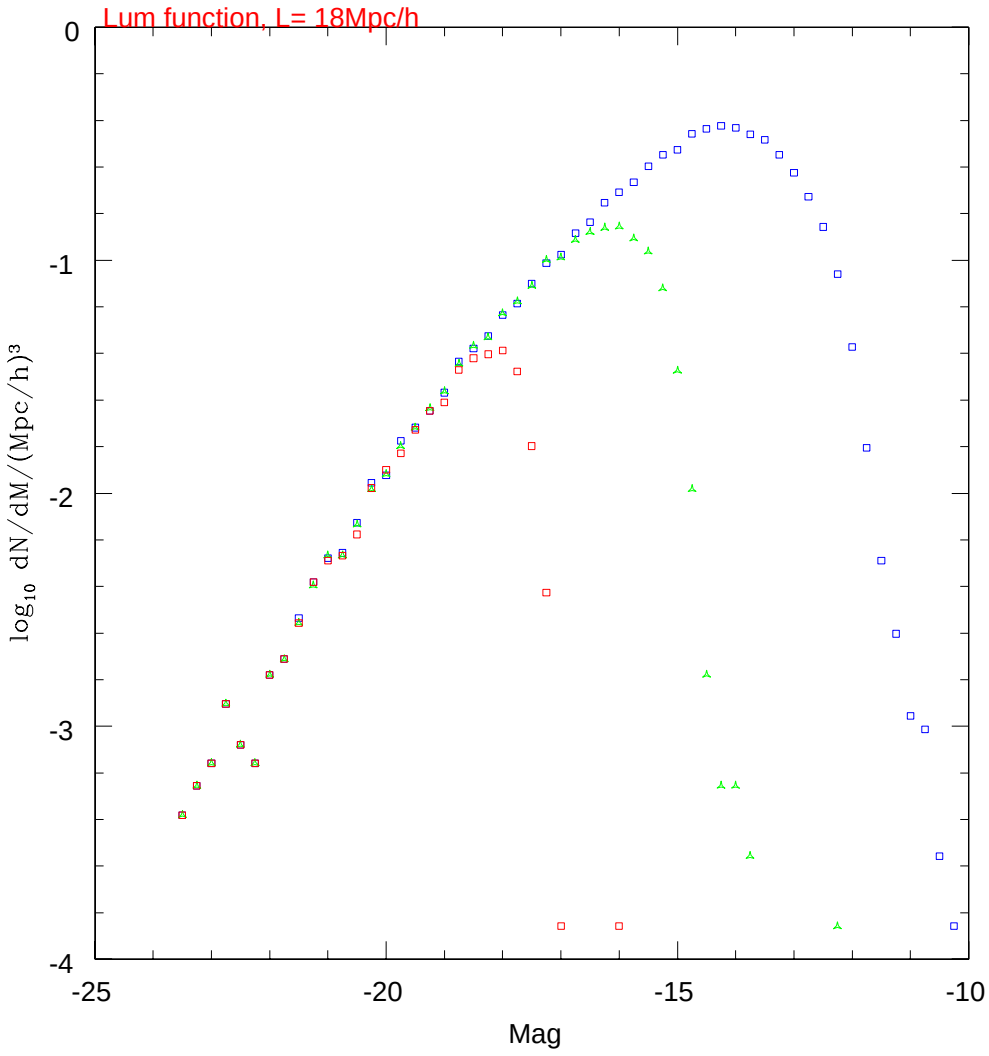

Figure 6.2: LF at mean redshift 7.16 in J Filter

Blue-minimal sky BG (mag 40) ; Green-very small BG (mag 30) ; Red-normal space sky BG (mag 22.6)

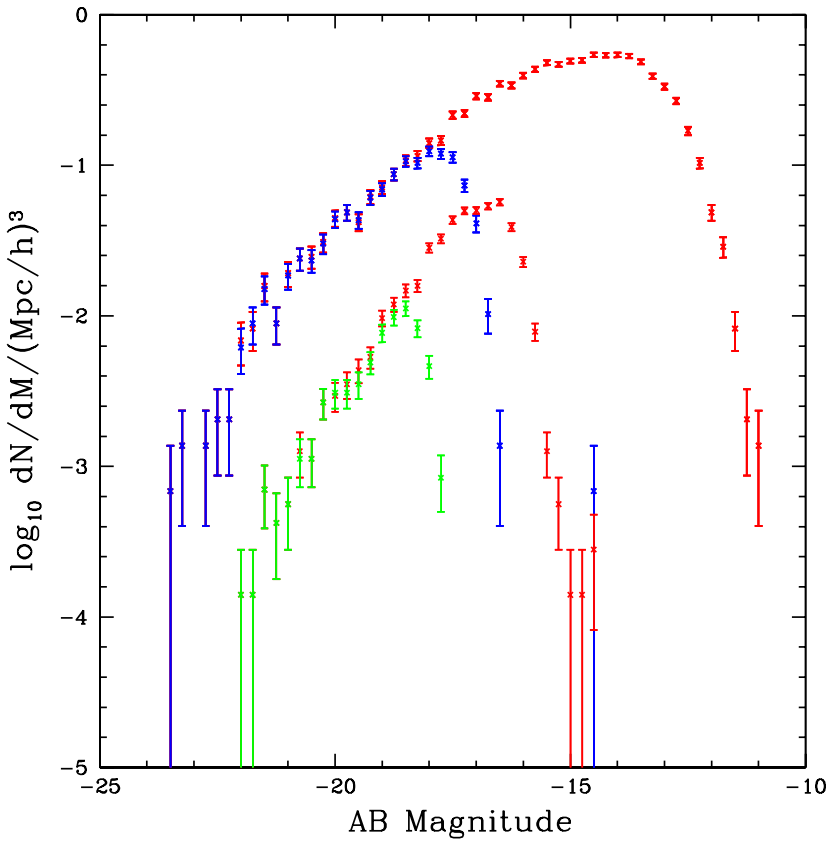

Figure 6.3: LF at mean redshifts 5.32
(upper left, z filter) and 9.50
(lower right, H filter)

1 sigma error bars ; alpha (5.32) : -1.70 +- 0.05 ; alpha (9.50) : -2.05 +- 0.10

various IR filters, described previously, and redshifts in the range of 4.5 to 11.0. The magnitudes are in the absolute AB system. The slope of the LF curves is fitted for $-25 \leq AB \leq -17$, except for redshift z greater than 8, where the fitting is for $-20 \leq AB \leq -18$ due to the fall-off at fainter magnitudes, the completeness limit. In order to test for the completeness limit, a series of fittings were taken, adjust the magnitude limit fainter by 0.5 magnitude increments. The minimum chi square fit was chosen. When the completeness limit was reached, the chi square value increased rapidly, so this seemed a fairly sharp division, and provided an objective measure of

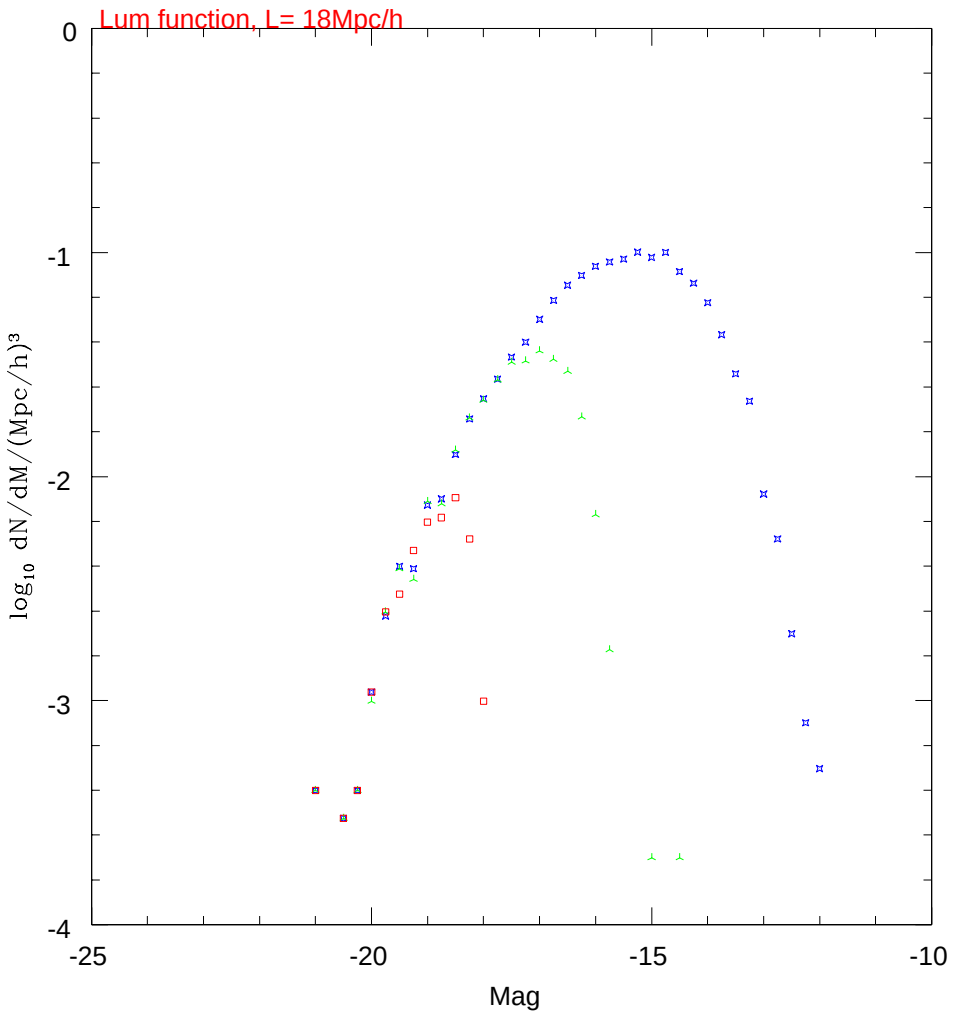

Figure 6.4: LF at mean redshift 10.87 in H Filter

Blue-minimal sky BG (mag 40) ; Green-very small BG (mag 30) ; Red-normal space sky BG (mag 22.6)

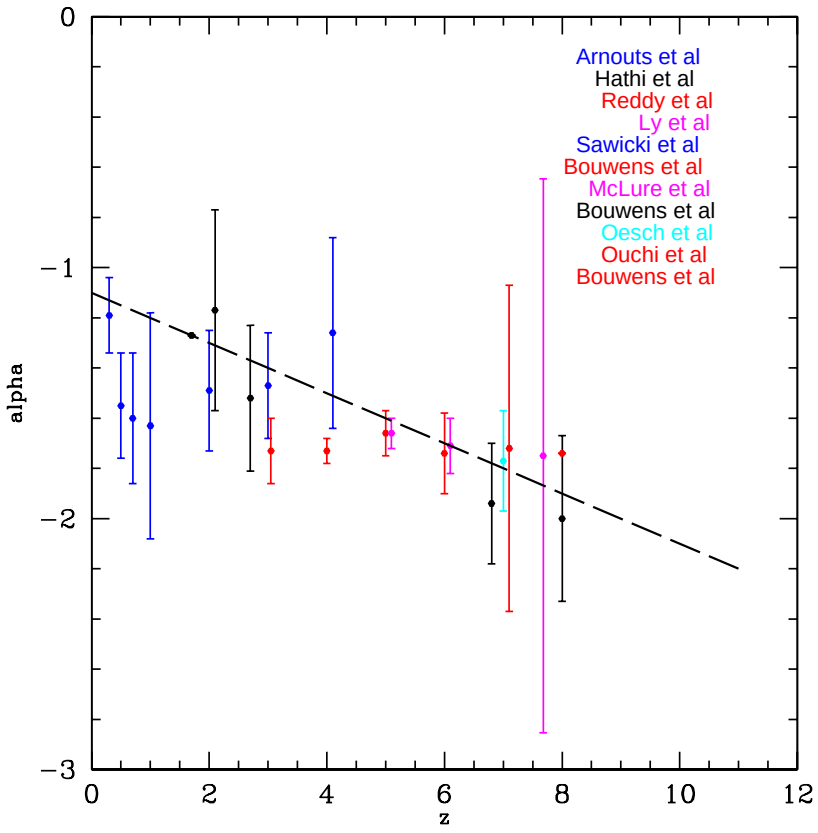

Figure 6.5: LF slope and observed alpha data
from Hathi, et al. (2010)

the limit. The figures are the LF's for minimal noise background (BG), of approximately 39-40 mAB. Figures are also shown for sky BG levels of $\sim$ 28 AB mag and more realistic sky BG of $\sim$ 22.6 AB mag and simulated exposures of $\sim$ 100 hours. These show the effects of increased noise on the completeness limit.

The slope gives the Schechter function parameter alpha(z), from Hathi et al., which is plotted as a function of redshift z in figures 7.6. Hathi et al. found alpha(z) = -1.10 - 0.10 $*$ z, using their data and other published data on the LF in the 150nm emission.

The simulation luminosity functions were fitted to a Schechter function using

minimization of the chi square and best fit to the Schechter function. The chi square fitting over the parameter space was used to obtain confidence intervals in the 2-D parameter space of $M*$ and slope alpha. Shown are contour plots of the chi square

values in alpha and M $*$ as well as fits of alpha of the LF to redshift z for both the no "WINDS" and "WINDS" (feedback) cases. Also shown are plots of alpha vs. redshift for realistic sky background noise for the no "WINDS" case, although this case has some problems at this time. The evolution of the LF slope alpha agrees well with the observational data reported in Hathi et al, for most of the range of their data, up to about redshift 6. with a fitted value of

$$\alpha = -1.066 \pm 0.026 - (0.113 \pm 0.005)z$$

However, for redshifts higher than 6.1, the alpha slope of the LF appears to level off with a range of about -1.7 to -1.9. Fitting alpha to redshift z in this range produces a fit of

$$\alpha = -1.51 \pm 0.064 - (0.038 \pm 0.009)z.$$

The addition of sky BG noise makes the analysis more difficult with larger errors and variances in the data. The overall fit over redshifts from 4.5 to 10.87, for a threshold of -18.7 M_AB for finding the completeness limit is:

$$\alpha = -1.085 \pm 0.212 - (0.108 \pm 0.035)z.$$

While this is comparable to the near no noise case, the fit is rather poor, with a reduced chi square value of 1.96 and a probability of only 0.044, below the normally accepted limit of 0.1. Much of this error is due to the high uncertainty at a redshift of z = 10.87. Also, the value of alpha was unstable, showing large changes in the fitting data. The value shown had a lower chi square than other values, but not that significantly. The data for this case calls for more careful analysis, perhaps averaging over different alpha values found when moving the window of the fit.

Removing the value at redshift 10.87, results in a somewhat better fit, though the probability is still only 0.079, still unsatisfactory. The fit then is

$$\alpha = -0.926 \pm 0.23 - (0.135 \pm 0.038)z.$$

The ”WINDS” simulation case shows a similar dependence of alpha on redshift, albeit with alpha values about 0.1 to 0.2 lower (more negative), especially at the high redshift end of 10.4. The fitted value was:

$$\alpha = -1.66 \pm 0.32 - (0.048 \pm 0.05)z$$

Note, however, this was for only one setting of model parameters, and (See discussion.)

Examination of the data files showed a suppression of star formation after about redshift 9 in the feedback (”winds”) output, relative to the no feedback (except for supernovae heating and metals) model. The ”winds” model was higher in star production initially, but the no feedback model passed it up around z of 9, and quickly outpaced it. This may account for the relatively high slope (alpha) of the LF in the ”winds” model, as there were fewer star ”particles” or clusters and galaxy ”building blocks” to merge and form larger numbers of galaxies at the more massive and brighter end of the LF.

Also shown, are the results of fitting the characteristic magnitude, M/ast, to the cases of no stellar winds, with and without sky BG, and the case of stellar winds (feedback.) There appears to be a general trend of brightening of the characteristic magnitude, M/ast, with redshift.

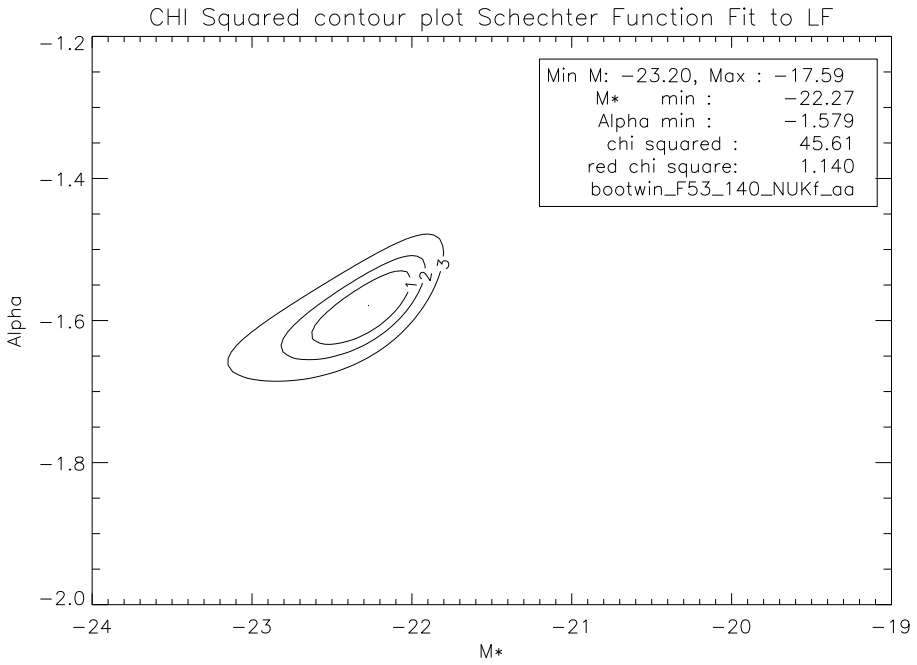

Figure 6.6: Confidence region plot of alpha vs M∗ , no “WINDS ”

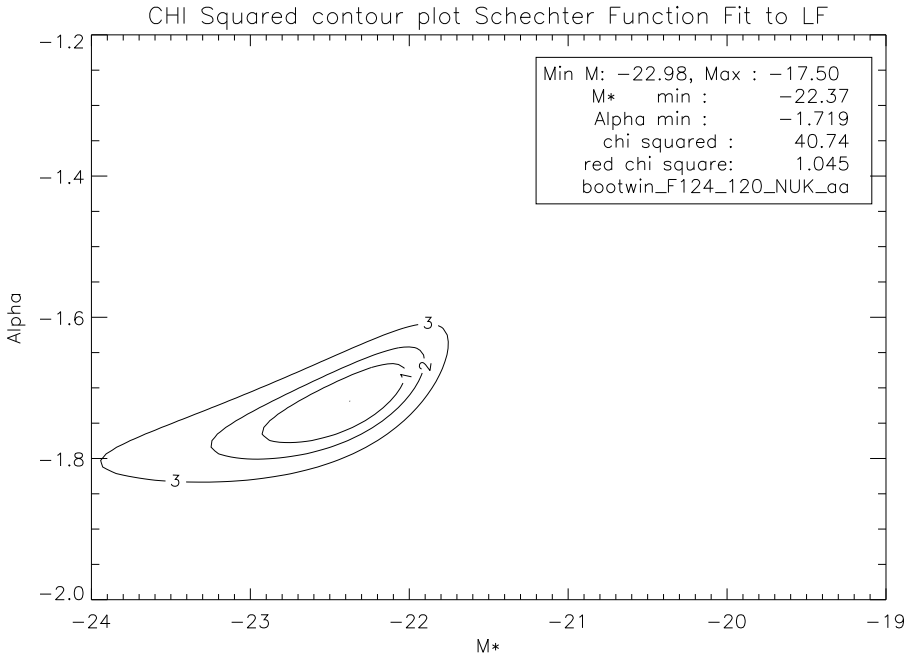

Figure 6.7: Confidence region plot of alpha vs M∗ , no “WINDS ”

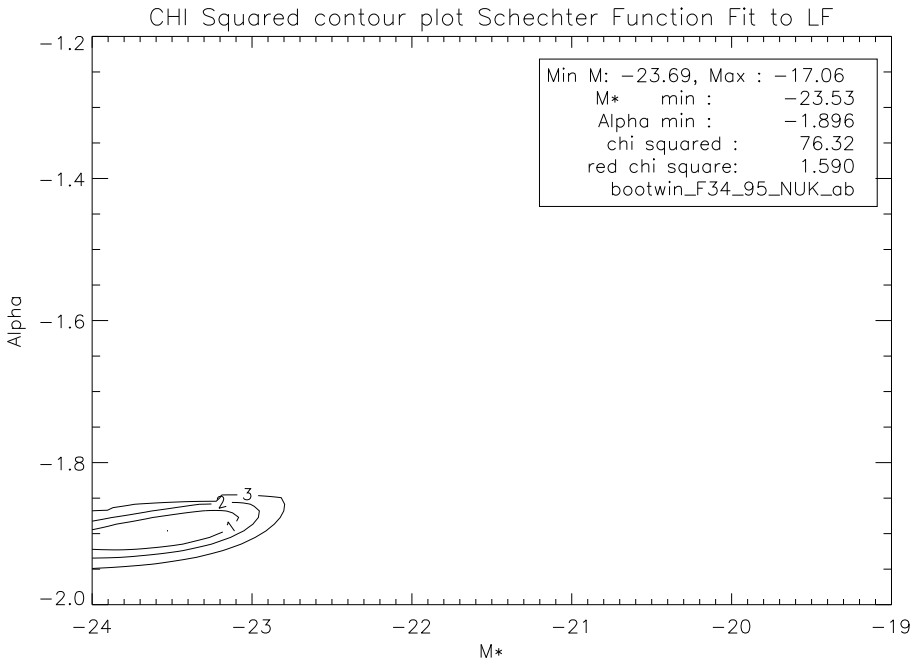

Figure 6.8: Confidence region plot of alpha vs M∗ , no “WINDS ”

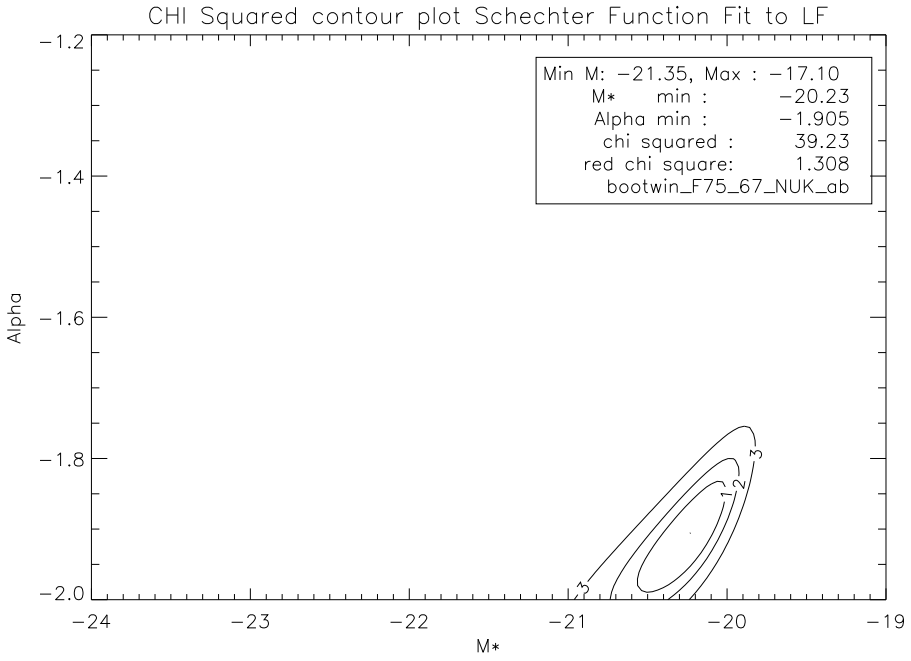

Figure 6.9: Confidence region plot of alpha vs M∗ , no “WINDS ”

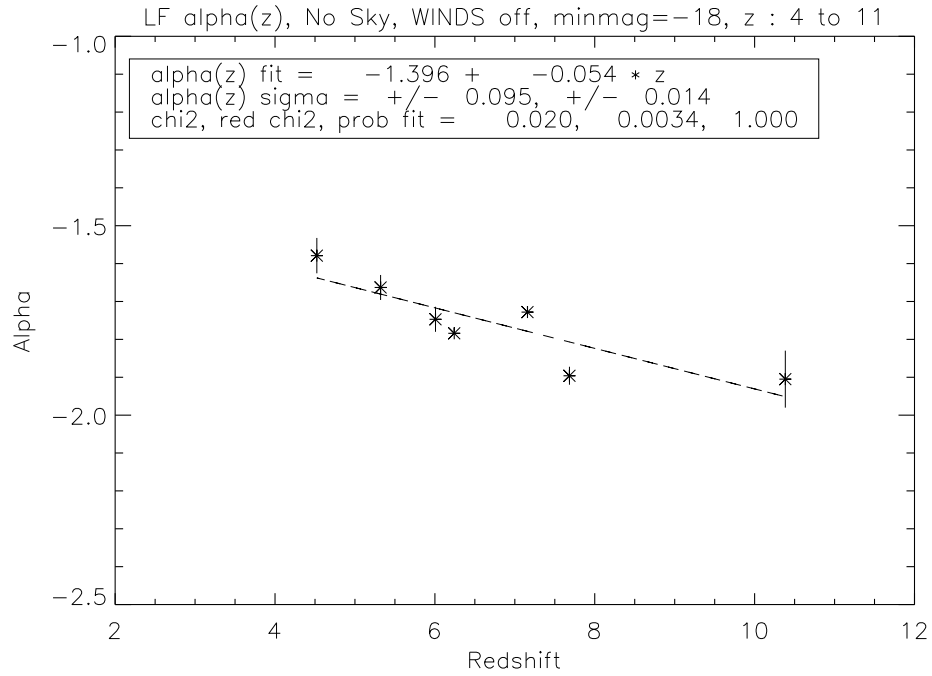

Figure 6.10: Simulated LF alpha vs. redshift
Sky BG $\sim$ 39 AB mag, no "WINDS"
$4.0 \leq z \leq 11$

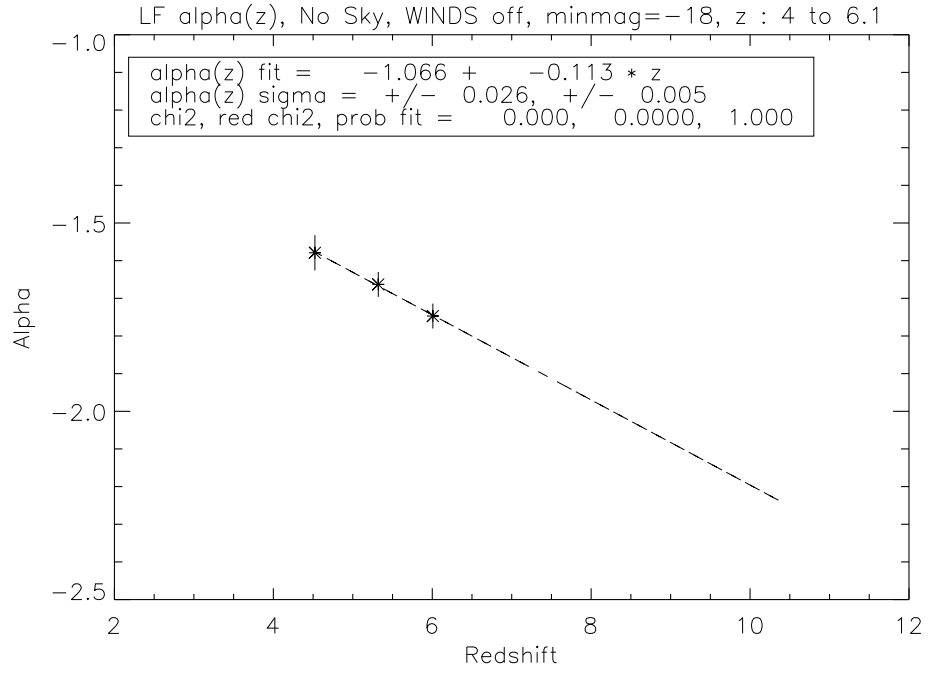

Figure 6.11: Simulated LF alpha vs. redshift
Sky BG $\sim$ 39 AB mag, no "WINDS"
$4.0 \leq z \leq 6.1$.

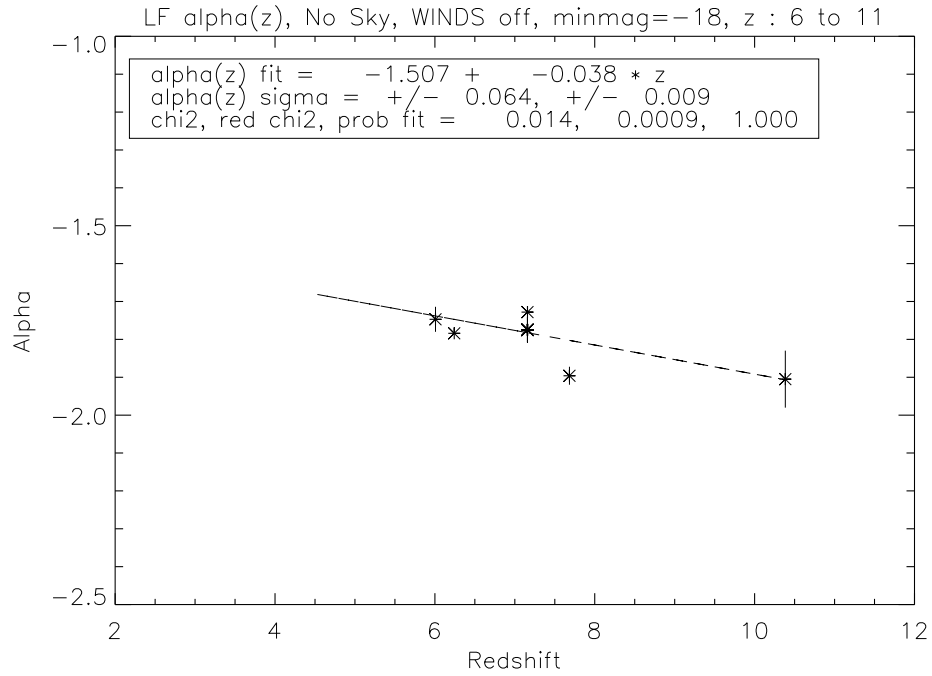

Figure 6.12: Simulated LF alpha vs. redshift
Sky BG $\sim$ 39 AB mag, no “WINDS”
6.0 $\leq$ z $\leq$ 11.0.

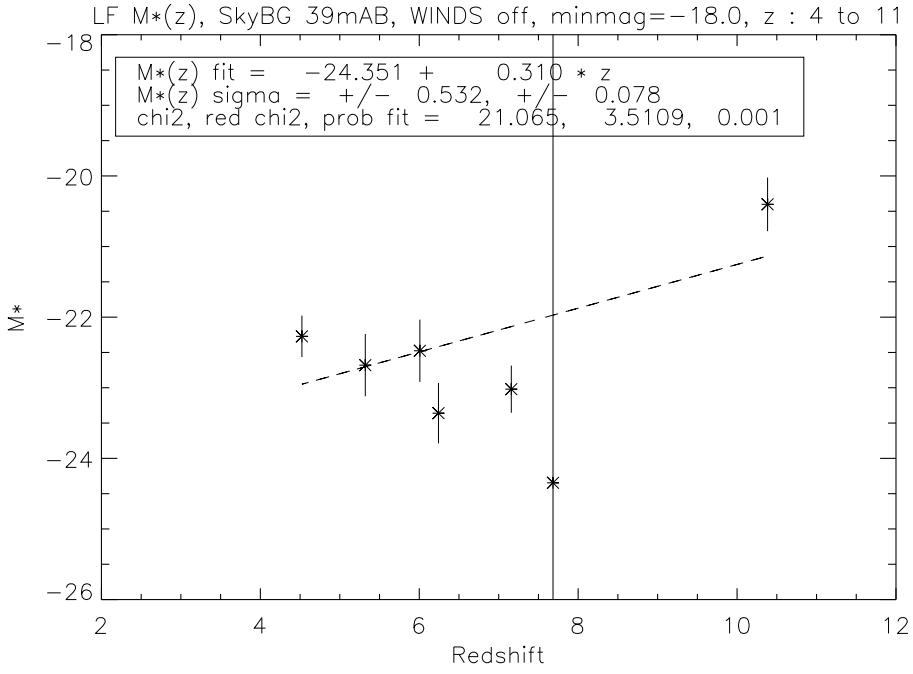

Figure 6.13: Simulated LF M$*$ vs. redshift,
Sky BG $\sim$ 39 AB mag, no ”WINDS”,
4.0 $\leq$ z $\leq$ 11.0.

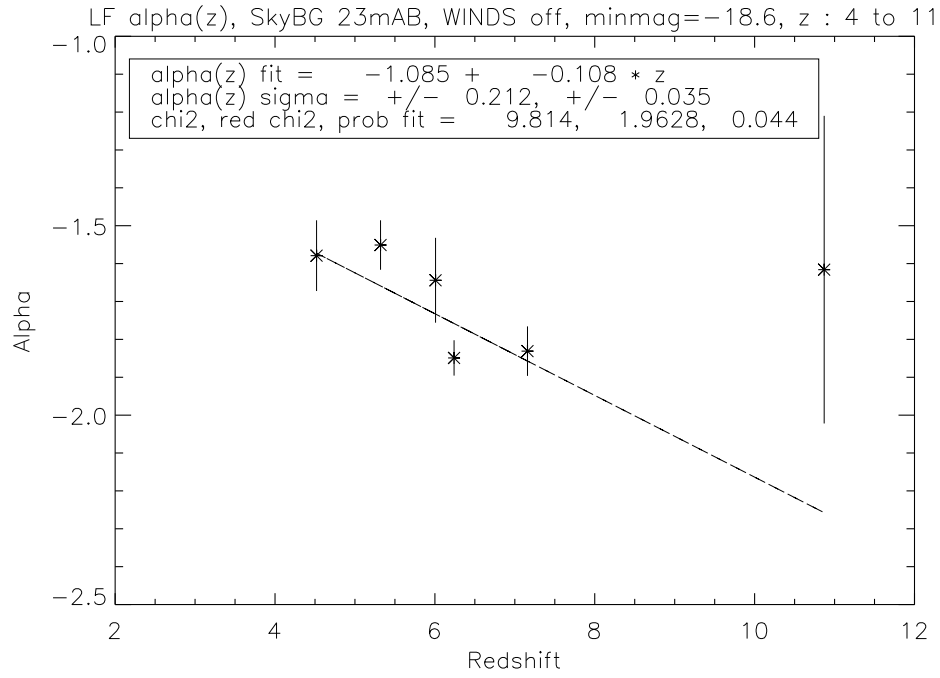

Figure 6.14: Simulated LF alpha vs. redshift,
Sky BG $\sim$ 23mAB, no ”WINDS”,
4.0 $\leq$ z $\leq$ 11

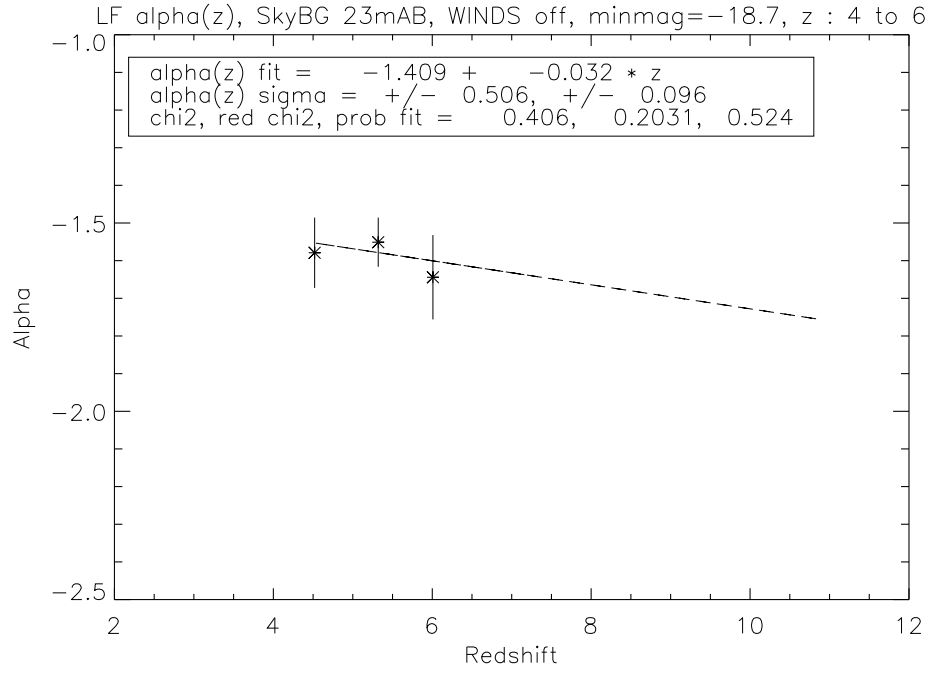

Figure 6.15: Simulated LF alpha vs. redshift,
Sky BG $\sim$ 23mAB, no “WINDS”,
4.0 $\leq$ z $\leq$ 6.1.

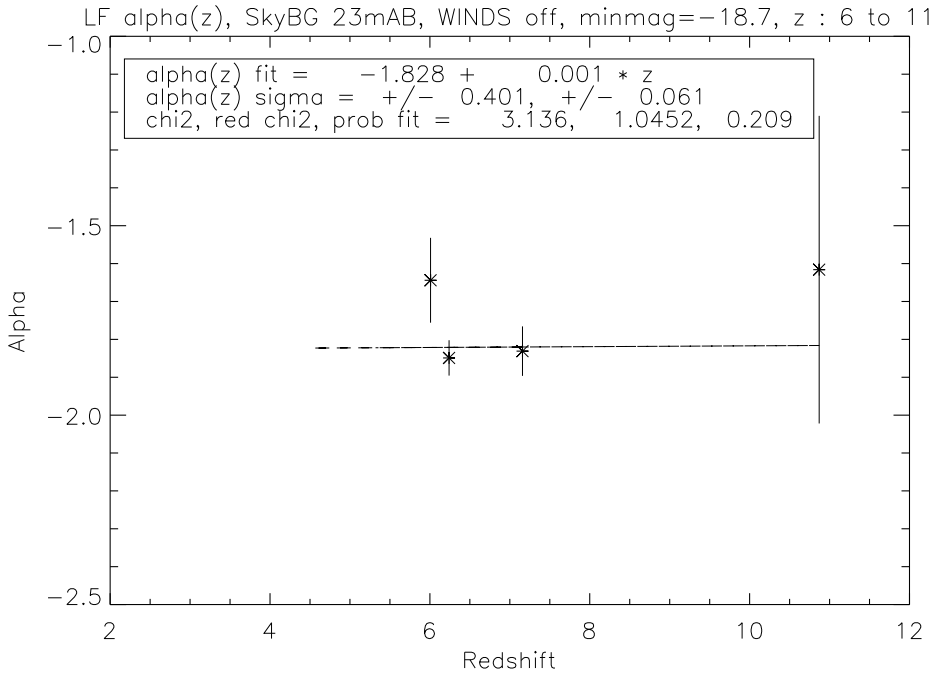

Figure 6.16: Simulated LF slope alpha vs. redshift,
Sky BG $\sim$ 23mAB, no “WINDS”,
$6.0 \leq z \leq 11.0$.

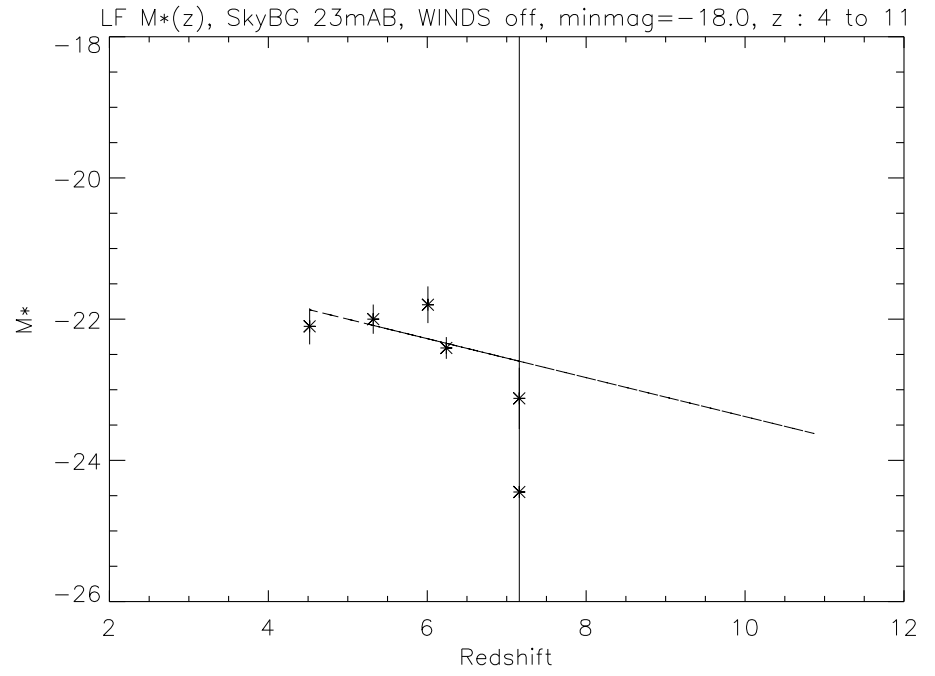

Figure 6.17: Simulated LF M$*$ vs. redshift,
Sky BG $\sim$ 22.6 AB mag, no ”WINDS”,
$4.0 \leq z \leq 11.0$.

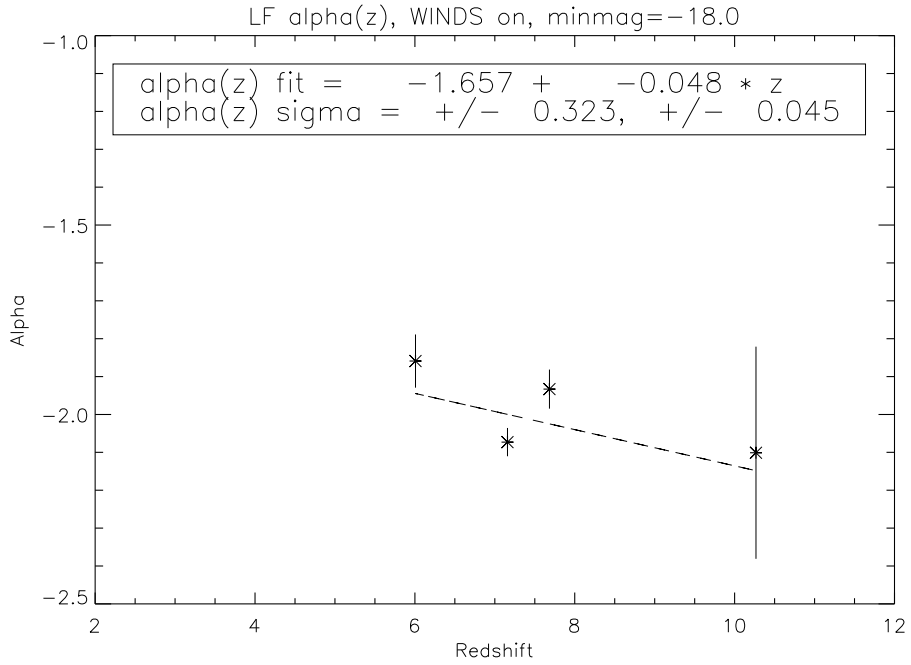

Figure 6.18: LF Schechter Fit alpha of
Simulation w/WINDS
mags fainter than 18.0 M_{AB}.

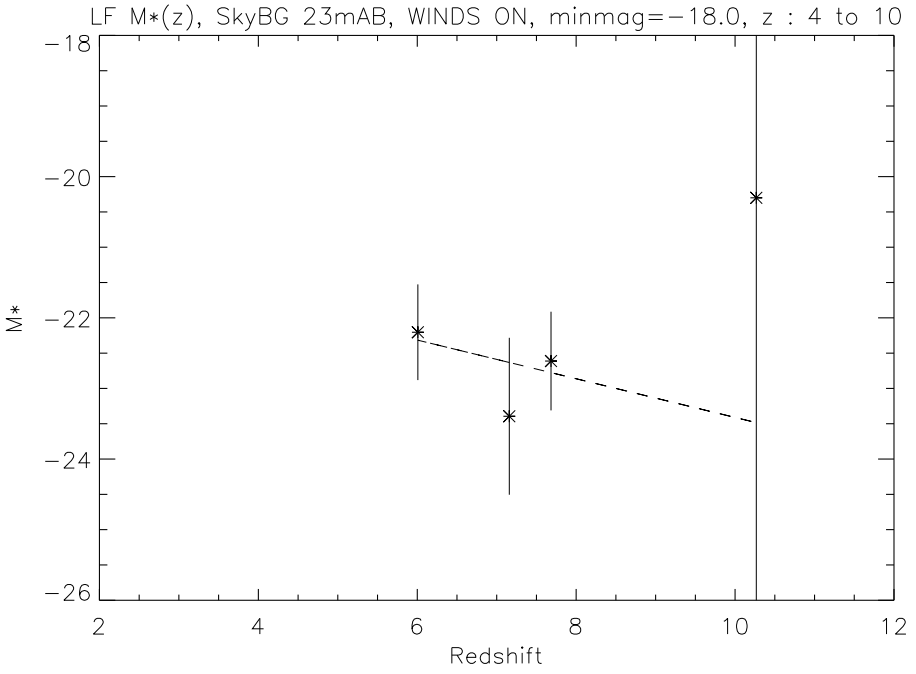

Figure 6.19: Simulated LF M$*$ vs. redshift,
Sky BG $\sim$ 39 AB mag, “WINDS” ON,
6.0 $\leq$ z $\leq$ 11.0.

6.2 Phi(M)

Normally, one is interested in the Schechter function normalization, $\phi*$. However, since this is dependent upon the value of the characteristic magnitude, M$*$, ($\phi(M*)$ = 0.921 * $\phi*$ * e^{-1}), and it has been shown that M$*$ is unreliable in this simulation due to the effects of the simulation box size on restricting the growth of massive, hence luminous, galaxies, it is better to consider the number density as a function of magnitude M, ϕ(M), the volume density of objects in the range M to M+dM.

Here, I compare ϕ(M) with recent data by Oesch, et al. (2012), herafter Oesch12, on the UV luminosity function at redshift z$\sim$8 from "CANDELS." Earlier data for lower redshifts is also considered. Following the data in Oesch12, I consider phi at M_{UV} of -20.1, and -17.7 and corresponding values when extinction is considered, below.

Comparing the data, without corrections for extinction, shows markedly higher values in the simulated data. However, this considers only the integrated output of stellar luminosity without radiative effects. In reality, dust reprocesses the stellar luminosity, especially in the UV, and re-radiates it, preferentially in the far IR (FIR) to sub-millimeter wavelengths. Further, there are obscuration effects, wherein regions of high luminosity are highly absorbed by dense regions of gas and dust (Nagamine, Cen and Ostriker (2000)). When these effects are taken into account, the simulation results are in better agreement with observed data. As before, AB magnitudes are used here.

From Bouwens. et al. (2011d), the J_{125}-H_{160} filters from WFC3 correspond to wavelengths of 174.1 nm at z$\sim$7 and 200.4 nm at z$\sim$6. Extrapolating, these filters would correspond to a restframe wavelength of 154.2 nm at z$\sim$8, a little longer than the restframe of 150 nm targeted in this study, but reasonably close. Since the CANDELS data in Oesch12 was limited, they combined results with that of Bouwens et al. (2011c) to obtain the UV LF.

I also look at the evolution of ϕ(M) at the -20.1, -18.94 and -17.7 AB mag levels with redshift. Note that ϕ(M) can show evolution with redshift, even if $\phi*$ shows little change. This is because, as noted previously, $\phi*$ depends upon $M*$, which shows evolution with redshift in observational data.

6.3 Extinction

Extinction and obscuration effects are taken from Nagamine, et al. (2000.) There, a simplified model of galaxy formation, including hydrodynamics, was used to calculated total stellar luminosities in the UV (150 nm and 280 nm ranges) by coupling to Bruzual-Charlot isochrone models (1999.) They estimated that a fraction f of the total UV luminosity was heavily obscured (optical depth, $\tau \geq 100$) by dust in and around the galaxy, especially in the galaxy core. Thus, only a fraction (1-f) of the total luminosity escaped. Further, this fraction was moderately extincted according to general extinction laws, using $\tau \sim 0.2$.

They applied this to the total stellar luminosity, not to just some portion of the galaxy population. They discuss different hypotheses (the two population model, etc.) Here, I am applying the extinction equally to all the objects. This may be considered as a limit. One could also try a Monte Carlo approach and heavily obscure some fraction f of the total galaxy population. As long as the effect is not magnitude dependent, applying the corrections uniformly seems a logical first approximation.

Nagamine, et al. (2000) used a value of 1-f = 0.35, corresponding to an extinction magnitude A = -2.5log(0.35) = 1.14. The moderate extinction (τ = 0.2) corresponds to an A_{UV} = -1.086 * $\tau \sim$ 0.2 mag. Here, I apply the moderate extinction correction separately and together with the obscuration factor to give a range of corrections, i.e., corrections of 0.2 mag and 1.34 mag.

From the table in Oesch12, we use the magnitudes -20.14, -18.94, and -17.74 for comparison with the corrections. This gives corrected magnitudes in the simulated

data of -20.34, -19.14 and -17.94 at the 0.2 correction level and -21.48, -20.28 and -19.08 at the 1.34 mag correction level. The simulated data is interpolated to give the counts at these magnitudes, and comparisons are made with simulated data at z=7.68 and z=10.38 with the the observed z $\sim$ 8 data.

6.4 Discussion of ϕ(M)

It is seen that the 1.34 AB mag correction at z = 10.38 appears to "overcorrect" the simulated data. However, this is at a redshift higher than the observed z $\sim$ 8 data, so the effect may be due to the early stages of growth, when ϕ is naturally less. Also, it can be argued that at this high redshift, there has been less time for dust to form, hence the obscuration factor may be less than that used here.

However, especially when viewing the highly corrected data, the Oesch12 ϕ(M), for M=-18.9, value at z $\sim$ 8 lies between the corrected simulation data at z = 7.68 and z = 10.38. However, when including data from Oesch12 for z $\sim$ 4 to 6, one notes that the simulated data shows a much higher value for ϕ. This is likely due to the lack of adequate feedback mechanisms in the model. One sees that the data with "WINDS" off is even higher, indicating that the feedback in the "WINDS" on model is having an effect. However, as noted previously, the lack of resolution in the model likely impacts the ability to adequately impact feedback.

Thus, we see a convergence at the higher redshifts of z $\geq$ 7, but evidence that the model is showing accelerated growth, compared with observed data, at lower redshifts. Also, while ϕ(M) shows evolution with redshift for reasons previously noted, one can see that if M is taken to be fainter with redshift, that ϕ(M) remains fairly constant.

Below are tables showing corrections for extinction (see text.) First table shows AB magnitude values corresponding to correction levels discussed in the

0 correction	0.2 AB mag	1.34 AB mag
-20.14	-20.34	-21.48
-18.94	-19.14	-20.28
-17.74	-17.94	-19.08

Table 6.1: Magnitudes for comparison, w/corrections.

0 correction	Oesch12 data	0	0.2	1.34
-20.14	0.097 +- 0.035	2.394 +- 0.35	1.833 +- 0.30	0.811 +- 0.203
-18.94	1.030 +- 0.35	7.508 +- 0.66	5.737 +- 0.56	2.092 +- 0.296
-17.74	4.520 +- 2.07	20.131 +- 0.99	17.885 +- 0.99	6.257 +- 0.558

Table 6.2: z = 7.68 simulation, WINDS ON, ϕ in 10^{-3} Mpc^{-3} mag^{-1}. No correction and corrections of 0.2 and 1.34 magnitudes for extinction. Compared with Oesch12 data.

previous section. Next two tables show ϕ(M) values from Oesch12 and corrected simulation data at redshifts 7.68 and 10.38 to bracket the Oesch12 data. Note that the simulated data is with the “WINDS” parameter ON.

		mags		
correction	Oesch12 data	0	0.2	1.34
-20.14	0.097	0.498 +- 0.153	0.231 +- 0.103 (-20.3)	N/A
-18.94	1.030	2.338 +- 0.339	1.733 +- 0.275	0.231 +- 0.103
-17.74	4.520	9.965 +- 0.73	8.217 +- 0.657	1.95 +- 0.275

Table 6.3: z=10.38 simulation, WINDS ON, ϕ in 10^{-3} Mpc^{-3} mag^{-1}. No correction and corrections of 0.2 and 1.34 magnitudes for extinction. Comapred with Oesch12 data.

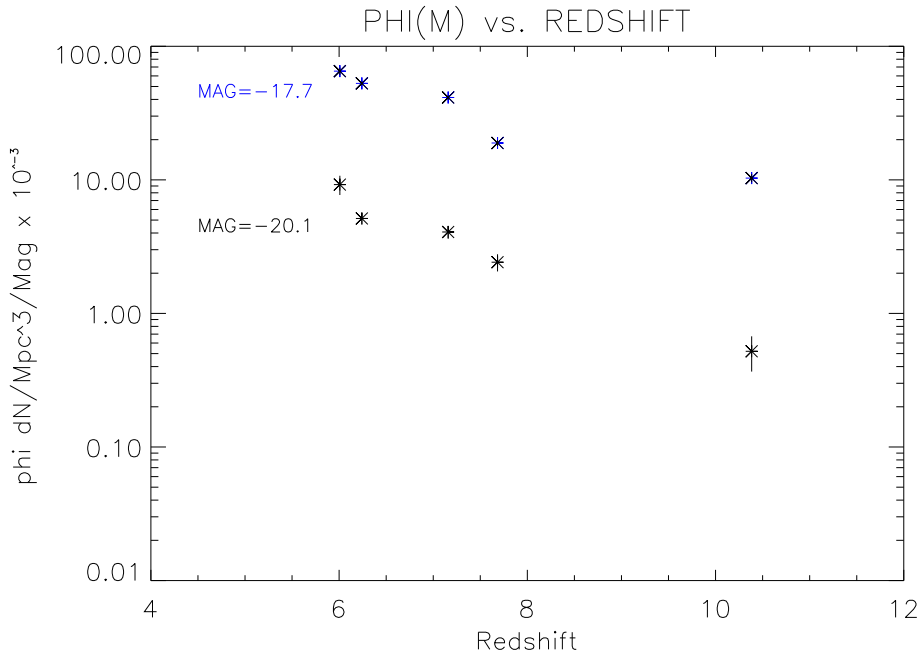

Figure 6.20: ϕ(M) dependence upon redshift
MAB= -17.7 and -20.1.
WINDS parameter ON.

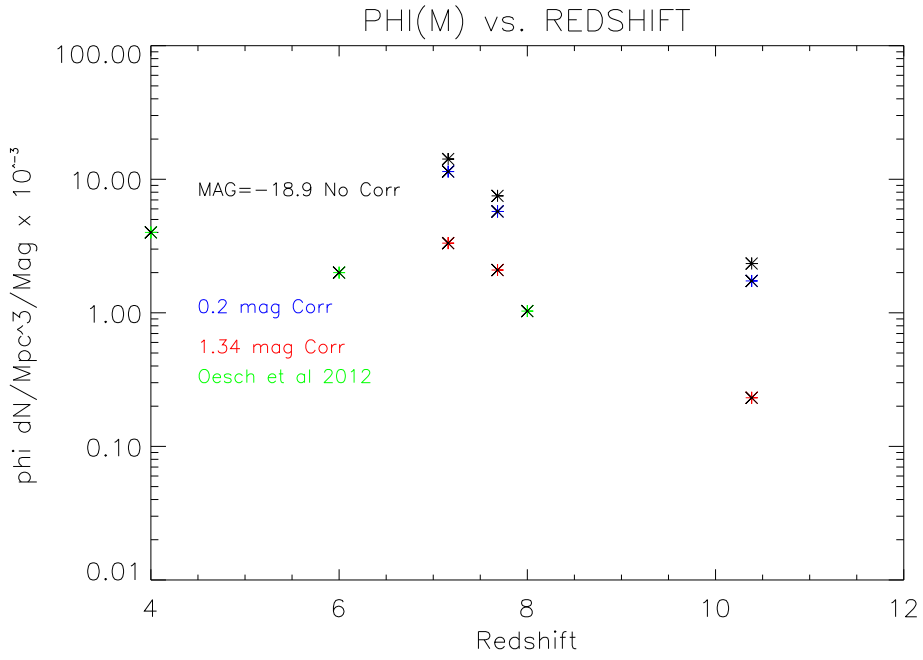

Figure 6.21: ϕ(M) at M=-18.94 (no correction) and
with extinction corrections of 0.2 and
1.34 AB mag compared with Oesch12
z $\sim$ 4 to 8

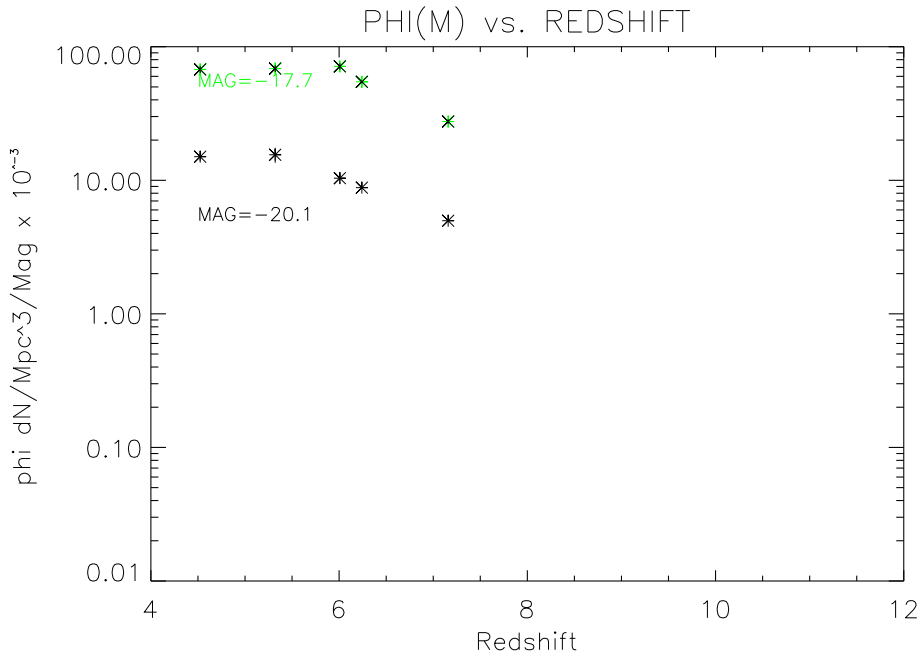

Figure 6.22: ϕ(M) dependence upon redshift,
M_{AB} = -17.7 and -20.1.
WINDS parameter OFF.

Chapter 7

CONCLUSIONS

This method of synthesis of observational techniques with numerical simulation appears promising for both evaluation of simulations and for aiding observational analysis and comparison with theory.

Values of the slopes of the LF functions from redshift 4.5 to $\sim$6.2 were consistent with observational data from Hathi, et al. with an alpha of $\sim$-1.6 to -1.7.

The evolution of the LF slope with redshift is consistent with Hathi, et al. up to about redshift 6, with a factor of about -0.1 of alpha with respect to redshift z in both cases. However, the simulation data shows a flattening of the redshift evolution after redshift 6, leveling off with an alpha of $\sim$ -1.6 to -1.8, with a factor of -0.04 of alpha with redshift z.

The case of incorporating feedback in the form of stellar and S/N winds shows a fairly flat evolution of the LF slope in the range of redshift greater than 6. Depending upon the selection of the completeness limit, one can obtain an evolution factor of $\sim$ -0.05, consistent with the no, or limited, feedback model case. However, alpha is much steeper in this case, in the range of $\sim$ -1.8 to -2.2.

Note, however, that this was for only one value of parameters and the resolution of gas particles in the model is probably too high for this level of physics. There is some evidence of a break at about M $\sim$ -22 to -23, a bit brighter than observations at lower redshifts.

Comparing ϕ(M) with observation, one finds a much steeper dependence on redshift in the simulated data. One also sees that ϕ(M) is generally much higher than published data. However, with corrections for extinction and obscuration by dust, the

simulated data appears to converge with observed results at z $\sim$ 7 to 8, especially when the feedback “WINDS” parameter is on. The simulated data shows a leveling off of ϕ(M) from z $\sim$ 8 to 11.

These effects are likely due to an inadequate modeling of feedback in the current models. Although one sees a closer correlation with observed data when the feedback WINDS parameter is on, the lack of mass resolution in the model acts to inhibit the full effect of feedback.

The relatively small size (18 Mpc/h comoving cube) limits structure growth on the high mass and high luminosity regime, hence determination of M$*$ was found unreliable. This also prevented a proper comparison of the normalization parameter, $\phi*$, which is highly dependent on M$*$. Hence, ϕ(M), with M $\gg$ M$*$ was used for comparisons with data. This is not a serious problem, since the focus of this research was on the properties of the faint end of the LF, and resolution at the high mass end was sacrificed for better resolution at the faint and low mass end.

There is an ongoing effort to investigate issues such as completeness limits to improve the robustness of this technique. There is also a continuing effort to improve the statistical analysis of the data, which is challenging, in part, due to the relatively large amounts of data.

In general, this technique of examining simulation data in a manner similar to observation appears promising and results appear consistent with some current observations showing an evolution in the luminosity function slope with redshift up to about 6. It will be interesting to see if better observations at redshifts greater than 6 show the decrease in evolution of alpha, and whether feedback effects produce an alpha closer to -2.

REFERENCES

Bertin, E., & Arnouts, S. 1996, A&AS, 117, 393

Black, J. H. 1981, MNRAS, 197, 553

Bouwens, R.J., Illingworth, G.D., Oesch, P.A., et al. 2011, arXiV:1105.2038v2

Bouwens, R.J., Illingworth, G.D., Oesch, P.A., et al. 2011b, arXiV:1109.0994

Bruzual, G. and Charlot, S. 2003, MNRAS z344,1000

Casey, C., Optimizing SExtractor Parameters for the Subaru MACS Field

Dahlen, Thomas, et al., 2007, ApJ, 654, 172

Dodelson,S. 2003, “Modern Cosmology” (Academic Press)

Katz,N., Weinberg, D., Hernquist, L. 1996, ApJSupplement 105, 19

Fukugita, M. et al., 1996, AJ, 111, 1748

Gingold, R. A., Monoghan,J J., 1977, MNRAS, 181, 375

Hathi, N. et al. ,2010, ApJ, 720, 1708

Herrera, C., 2012, Turbulence in Cosmic Structure Formation, ASU

Hogg, D. W., et al., 2002, The K correction, ArXiv:astro-ph/0210394

Longair, Malcom S., Galaxy Formation, Springer, 1998

Lucy, L. 1977, AJ, 82, 1013

Nagamine, K., Cen, R., Ostriker, J. P., 2000, ApJ, 541, 25

Nagamine, K. 2007, AAS...21010702N

Oesch, P. A., Bouwens, R.J., Illingworth, G.D., et al., arXiv:1201.0755v1

Oke, J. B., and Gunn, J. E., 1983, ApJ, 266, 713

Overzier, et al. 2012, AAS Winter 2012 Meeting

Phillipps, Steven, The Structure & Evolution of Galaxies, Wiley, 2005

Sparke, L. S., & Gallagher, J. S. III, Galaxies in the Universe

Springel, V. 2000, MNRAS 312, 859

Springel, V. 2005, MNRAS 364, 1105

Springel,V. and Hernquist, L. 2002, MNRAS 333, 649

Springel,V. and Hernquist, L. 2003, MNRAS 339, 289

Wall, J.V., Jenkins C.R., Practical Statistics for Astronomers, Cambridge University Press, 2003

Windhorst, R. A. 2009, Astro2010S , 317

Wright 2006, PASP, 118, 1711